IEEE Access
Multidisciplinary | Rapid Review | Open Access Journal

Received January 19, 2021, accepted January 29, 2021, date of publication February 2, 2021, date of current version February 10, 2021.

Digital Object Identifier 10.1109/ACCESS.2021.3056423

Optimal Reactive Power Dispatch With Time-Varying Demand and Renewable Energy Uncertainty Using Rao-3 Algorithm

MOHAMED H. HASSAN[1], SALAH KAMEL[1], MAHMOUD A. EL-DABAH[2], TAHIR KHURSHAID[3], (Member, IEEE), AND JOSÉ LUIS DOMÍNGUEZ-GARCÍA[4], (Member, IEEE)

[1]Department of Electrical Engineering, Faculty of Engineering, Aswan University, Aswan 81542, Egypt
[2]Electrical Engineering Department, Faculty of Engineering, Al-Azhar University, Cairo 11651, Egypt
[3]Department of Electrical Engineering, Yeungnam University, Gyeongsan 38541, South Korea
[4]Catalonia Institute for Energy Research (IREC), 08930 Sant Adrià de Besòs, Spain

Corresponding authors: Tahir Khurshaid (tahir@ynu.ac.kr), Mahmoud A. El-Dabah (dr_mdabah@azhar.edu.eg), and Salah Kamel (skamel@aswu.edu.eg)

ABSTRACT The appropriate control and management of reactive power is of great relevance in the electrical reliability, stability, and security of power grids. This issue is considered in order to increase system efficiency and to maintain voltage under the acceptable value range. In this regard, novel technologies as FACTS, renewable energies, among others, are varying conventional grid behavior leading to unexpected limit capacity reaching due to large reactive power flow. Thus, optimal planning of this must be considered. This paper proposes a new application for a simple and easy implementation optimization algorithm, called Rao-3, to solve the constrained non-linear optimal reactive power dispatch problem. Moreover, the integration of solar and wind energy as the most applied technologies in electric power systems are exploited. Due to the continuous variation and the natural intermittence of wind speed and solar irradiance as well as load demand fluctuation, the uncertainties which have a global concern are investigated and considered in this paper. The proposed single-objective and multi-objective deterministic/stochastic optimal reactive power dispatch algorithms are validated using three standard test power systems, namely IEEE 30-bus, IEEE 57-bus, and IEEE 118-bus. The simulation results show that the proposed optimal reactive power dispatch algorithms are superior compared with two recent algorithms (Artificial electric field algorithm (AEFA) and artificial Jellyfish Search (JS) algorithm) and other optimization algorithms used for solving the same problem.

INDEX TERMS Renewable energy, uncertainty, time-varying demand, optimal reactive power dispatch (ORPD), RAO algorithm, backward reduction algorithm.

I. INTRODUCTION

Optimal reactive power dispatch (ORPD) is considered one of the most very important conditions for the secure and economic operation of power systems. It is achieved by suitable coordination of the system equipment used to manage the reactive power flow with the aim of minimizing the active power losses and/or improving the voltage profile of the system.

The ORPD aims at the control and management of reactive power to minimize total active power loss, and a total of voltage deviations, and the voltage stability margin improvement while preserving equality and inequality constraints within their acceptable limits [1], [2]. The active power losses are set as an objective in the ORPD problem. In order to achieve the desired objective, the generator bus voltages, settings of passive devices such as transformers and shunt VAR compensators are adjusted to reduce the active power losses. The cumulative sum of voltage deviations of load buses is also set as an objective. The purpose of this objective is to ensure that voltages at consumer terminals are closed to the required level (usually from 0.95 to 1.1 p.u.) with control of reactive power flow. The ORPD problem is a nonlinear complex optimization problem. These types of non-convex and

The associate editor coordinating the review of this manuscript and approving it for publication was Jagdish Chand Bansal.

non-linear optimization problems can be solved by classical methods such as Newton-Raphson [3], the interior point [4], linear programming (LP) [5], non-linear programming [6], and Quadratic programming (QP) [7]. These classical methods suffer from massive computation, local optimal trapping especially when it is used in large-scale systems [8].

Metaheuristic techniques are more suitable than classic methods in solving non-linear optimization problems like ORPD. There are many metaheuristic optimization techniques were used to find the best solution for the ORPD problem such as; Whale Optimization Algorithm (WOA) [9], Particle Swarm Optimization (PSO) [10], Ant Lion Optimizer (ALO) [11], Improved Social Spider Optimization Algorithm (ISSO) [12], Improved Antlion Optimization Algorithm (IALO) [13], Genetic Algorithm (GA) [14], Ant Colony Optimizer (ACO) [15], Opposition-Based Gravitational Search Algorithm (OGSA) [16], Wind Driven Optimization Algorithm (WDO) [17], modified differential evolution algorithm (MDEA) [18], Specialized Genetic Algorithm (SGA) [19], evolutionary programming [20], comprehensive learning particle swarm optimization [21], fuzzy adaptive PSO (FAPSO) [22], seeker optimization algorithm (SOA) [23], cuckoo search algorithm (CA) [24], Hybrid Evolutionary Programming (HEP) [25], harmony search algorithm [26], Teaching Learning-Based Optimization [27], biogeography-based optimization [28], modified sine cosine algorithm [29], water cycle algorithm [30], hybrid Fuzzy-Jaya optimizer [31].

In [32], Moth Swarm Algorithm (MSA) has been used for ORPD considering the stochastic of renewable energy generation and load. The ORPD problem considering load uncertainty has been solved using an enhanced grey wolf optimizer (EGWO) in [33]. ORPD with uncertainties in load demand and renewable energy sources has been solved based on SHADE algorithm [34], Fractional Calculus with Particle Swarm Optimization Gravitational Search Algorithm (FPSOGSA) [35], and improved lightning attachment procedure optimization (ILAPO) [36]. In [37], Marine Predators Algorithm (MPA) has been used for solving ORPD problems with time-varying load, wind, and solar energy uncertainties. In [38], an enhanced firefly algorithm has been introduced for multi-objective optimal active/reactive power dispatch with uncertainties consideration. Also, in [39] a quantum-behaved particle swarm optimization differential mutation (QPSODM) algorithm is used to solve the multi-objective ORPD with renewable energy uncertainty. From an environmental, economic, and technical point of view, the switch from fossil-fueled-based generation to renewable energy sources is a must. This integration leads to reducing greenhouse emissions, generation fuel cost, and enhancing the system operation. The most applied technologies for RES are the wind and solar energy generation systems. Due to the continuous variation and the natural intermittence of wind speed and solar irradiance, moreover, load demand fluctuation there is an increasing concern of uncertainties of electrical power systems [40]. As it is a strenuous duty for effective planning, there are many approaches for modeling system uncertainty comprising probabilistic methods [41], possibilistic methods [42], hybrid possibilistic –probabilistic methods [43], robust optimization [44]. A comprehensive review of the stochastic techniques which have been implemented for the optimization of solar-based renewable energy systems has been presented in [45]. Moreover, Ref. [46] has considered the uncertainty of the renewable distributed generators for the management of battery energy storage employing a double deep Q-learning method. Analyzing the interdependency of natural gas, coal, and electricity infrastructures considering their operation constraints and wind power uncertainties using a robust optimization model has been introduced in [47].

The significant contributions of this research can be summarized as follows:

- Solving ORPD problem considering uncertain wind, and PV energy resources and time-varying load.
- Applying the Monte-Carlo simulation method for coping with many scenarios considering load, solar irradiance, and wind speed uncertainties.
- Proposing a new application for the Rao-3 algorithm for solving the ORPD problem with and without RES.
- Comparing the performance of the Rao-3 algorithm with the recent techniques for solving the ORPD problems.
- A comprehensive investigation of the deterministic and stochastic OPRD problem with compliance with all constraints.
- A single and multi-objective stochastic optimization framework for the ORPD problem.
- The results show the superiority of proposed optimal reactive power dispatch algorithms based on three standard test power systems.

The rest of this manuscript is structured as follows; the mathematical formation of ORPD is presented in Section II. Section III presents the mathematical equations for representing the uncertainties of load demand and RES. Section IV presents the developed ORPD algorithm based on the RAO-3 optimizer for solving the ORPD problem. Section V presents the main obtained results and discussion. The conclusion drawn from this research is introduced in Section VI.

II. PROBLEM FORMULATION

In this section, the mathematical formulation of the ORPD as an optimization problem will be presented. The objective function F of ORPD can be generally formulated as follows:

$$MinF(x, u) \tag{1}$$

$$\text{Sub. to } g_k(x, u) = 0 \quad k = 1, 2, \ldots, m \tag{2}$$

$$h_n(x, u) \leq 0 \quad n = 1, 2, \ldots, p \tag{3}$$

where, x, u represent the state and control variables vectors, respectively. The state vector comprises slack bus real power, load bus voltage, generators reactive power, and transmission line apparent power flow. On the other hand, generators' bus voltage, injected reactive power of compensator and

transformers tap setting constitute the control variable vector. The state and control variables vectors are given as:

$$x^T = [P_1, V_L, Q_G, S_T] \quad (4)$$
$$u^T = [V_G, Q_C, T_P] \quad (5)$$

A. OBJECTIVE FUNCTIONS

As mentioned previously, the ORPD mainly aims at finding the optimal working point of a given power grid. In this paper, two objectives functions are used to achieve this goal as follows:

i. Active power loss minimization:

$$F_1 = P_{Loss} = \sum_{i=1}^{N_L} G_{ij}\left(V_i^2 + V_j^2 - 2V_iV_j\cos\delta_{ij}\right) \quad (6)$$

ii. Voltage deviation minimization:

$$F_2 = VD = \sum_{i=1}^{N_Q} |V_i - 1| \quad (7)$$

where, V_i is the voltage of bus i, G_{ij} is line $i-j$ conductance and δ_{ij} is the voltage phase difference. While reaching the optimal operating point of a power system based on the previous objective functions, the equality and inequality constraints given by (8)-(16) must not be violated.

$$P_{GK}^{Min} \le P_{GK} \le P_{GK}^{Max} \quad K = 1, 2, \ldots, N_G \quad (8)$$
$$Q_{GK}^{Min} \le Q_{GK} \le Q_{GK}^{Max} \quad K = 1, 2, \ldots, N_G \quad (9)$$
$$V_{GK}^{Min} \le V_{GK} \le V_{GK}^{Max} \quad K = 1, 2, \ldots, N_G \quad (10)$$
$$T_n^{Min} \le T_n \le T_n^{Max} \quad n = 1, 2, \ldots, N_Q \quad (11)$$
$$Q_{cn}^{Min} \le Q_{cn} \le Q_{cn}^{Max} \quad n = 1, 2, \ldots, N_Q \quad (12)$$
$$S_{Ln} \le S_{Ln}^{Min} \quad n = 1, 2, \ldots, N_Q \quad (13)$$
$$V_n^{Min} \le V_n \le V_n^{Max} \quad K = 1, 2, \ldots, N_Q \quad (14)$$
$$P_{Gi} - P_{Li} = V_i \sum_{j=1}^{N_b} V_j\left(G_{ij}\cos\delta_{ij} + B_{ij}\sin\delta_{ij}\right) \quad (15)$$
$$Q_{Gi} - Q_{Li} = V_i \sum_{j=1}^{N_b} V_j\left(G_{ij}\sin\delta_{ij} - B_{ij}\cos\delta_{ij}\right) \quad (16)$$

The multi-objective functions are handled using the weighted sum approach as given in (17):

$$F = F_i + k_1\left(Q_{Gi} - Q_{Gi}^{lim}\right)^2 + k_2\left(V_{Li} - V_{Li}^{lim}\right)^2 + k_3\left(S_{Li} - S_{Li}^{lim}\right)^2 \quad (17)$$

where, k_1, k_2, k_3 are the penalty factors, while x^{lim} can be determined from the following equation:

$$x^{lim} = \begin{cases} x^{max} & if\ x > x^{max} \\ x^{min} & if\ x < x^{min} \end{cases} \quad (18)$$

However, the penalty factors usually depend on the optimization problem and their values are selected by trial and error approach [48]. The effect of the choice of these penalty factors in the case of solving the optimal reactive power dispatch problem has been studied in [48]. The study recommended the weight factor values to be $k_1 = 10$, $k_2 = 5$ and $k_3 = 5$ [48]. Hence, these values are used in the current paper.

III. LOAD DEMAND AND RES UNCERTAINTIES

The continuous probability density function (PDF) is utilized to incorporate the uncertainties in loads demand, wind, and solar energy as:

A. MODELING THE SPEED WIND UNCERTAINTY

Weibull PDF can be applied for the wind speed uncertainty modeling as [49]:

$$f_v(v) = \left(\frac{\beta}{\alpha}\right)\left(\frac{v}{\alpha}\right)^{(\beta-1)} exp\left[-\left(\frac{v}{\alpha}\right)^{\beta}\right] 0 \le v < \infty \quad (19)$$

where, α, β are the Weibull PDF scaling and shaping parameters. Figure 1 shows the 1000 Monte-Carlo wind speed distribution scenario utilizing Weibull PDF.

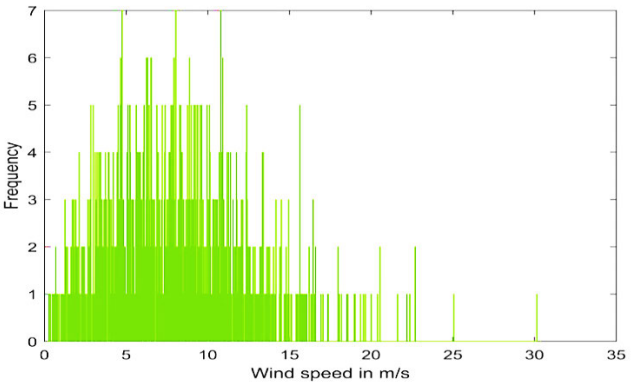

FIGURE 1. A 1000 Monte-Carlo wind speed distribution scenario utilizing Weibull PDF ($\alpha = 9$, $\beta = 2$) for the wind generator at bus 5.

As a function of wind speed, wind turbine output power can be determined as follows [50]:

$$P_\omega(v_\omega) = \begin{cases} 0 & for\ v_\omega < v_{\omega i}\ \&\ v_\omega > v_{\omega o} \\ P_{\omega r}\left(\frac{v_\omega - v_{\omega i}}{v_{\omega r} - v_{\omega i}}\right) & for\ (v_{\omega i} \le v_\omega \le v_{\omega r}) \\ P_{\omega r} & for\ (v_{\omega r} \le v_\omega \le v_{\omega o}) \end{cases} \quad (20)$$

where, $P_{\omega r}$ is the wind turbine rated output power ($P_{\omega r} = 3$W), $v_{\omega i} = 3\ m/s$, $v_{\omega o} = 25\ m/s$ and $v_{\omega r} = 16\ m/s$, are the wind turbine cut-in, cut-out, and the rated speeds, respectively. In this paper, the wind farm consists of 25 wind turbines, and the total output power is 75 MW.

The probability of wind speed for each wind scenario is calculated using (21).

$$\tau_{wind,k} = \int_{v_k^{min}}^{v_k^{max}} f_v(v)\, dv \quad (21)$$

where, v_k^{min}, v_k^{max} denote the starting and ending points of wind speed's interval at k^{th} scenario, $\tau_{wind,k}$ is the probability of the wind speed being in scenario k.

B. SOLAR IRRADIANCE UNCERTAINTY MODELING

Formulation of the solar irradiance uncertainty can be attained using the lognormal PDF as [51]:

$$f_G(G) = \frac{1}{G\sigma_s\sqrt{2\pi}} exp\left[-\frac{(\ln G - \mu_s)^2}{2\sigma_s^2}\right] \quad for\ G > 0 \tag{22}$$

where, σ_s, μ_s are the stranded deviation and the mean of the random variables which are selected to be equal to 0.5 and 5.5, respectively [34].

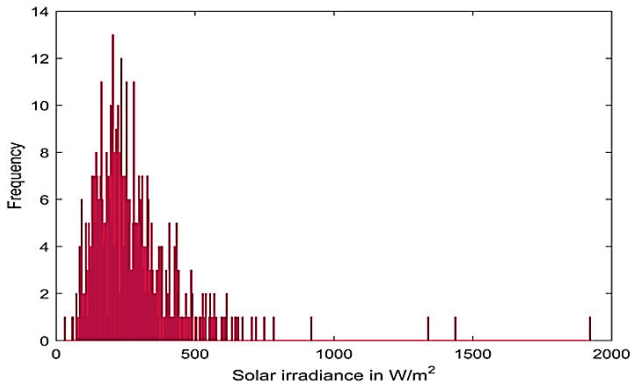

FIGURE 2. PV unit solar irradiance scenarios (without zero irradiance).

Figure 2 shows the solar irradiance scenarios employing the Monte-Carlo simulation. Due to sun unavailability during half of the daytime, the initialization of zero irradiance with 50% is used. While the remaining 50% probability covers the scenarios of solar irradiance generated using lognormal distribution mean $\mu_s = 5.5$ and standard deviation $\sigma_s = 0.5$.

The PV array output power as a function of irradiance can be calculated as [52]:

$$P_s(G) = \begin{cases} P_{sr}\left(\dfrac{G^2}{G_{std} \times X_c}\right) & for\ 0 < G \le X_c \\ P_{sr}\left(\dfrac{G}{G_{std}}\right) & for\ G \ge X_c \end{cases} \tag{23}$$

where, G_{std} is the standard solar irradiance which equals 1000 W/m^2 while, X_c denotes a certain irradiance point which is set as 120 W/m^2 [34]. P_{sr}, is the PV array output power which equals 50 MW in this paper.

Calculating the solar irradiance probability could be attained from [53]:

$$\tau_{solar,m} = \int_{G_m^{min}}^{G_m^{max}} f_G(G)\, dG \tag{24}$$

C. UNCERTAINTY MODELING OF LOAD DEMAND

The normal distribution PDF can be used to represent load modeling uncertainty as [54]:

$$f_d(P_d) = \frac{1}{\sigma_d\sqrt{2\pi}} exp\left[-\frac{(P_d - \mu_d)^2}{2\sigma_d^2}\right] \tag{25}$$

where, μ_d and σ_d are the mean and standard deviation values, respectively. While P_d denotes the probability density of load normal distribution. Load demand Monte- Carlo scenarios created using normal distribution PDF (sample size 1000, $\mu_d = 70$, $\sigma_d = 10$) as shown in Figure 3.

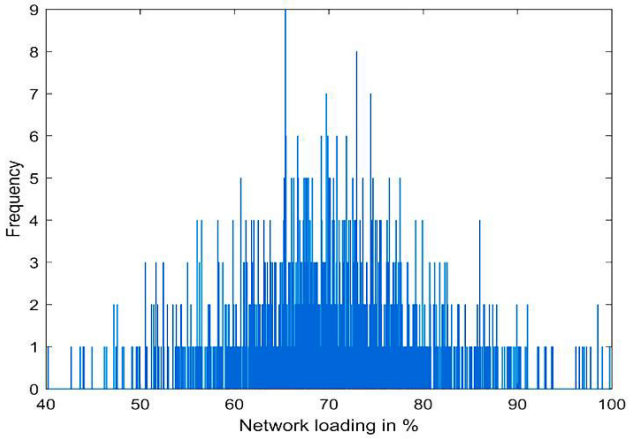

FIGURE 3. Monte-Carlo simulation of demand scenarios.

Load demand probability and expected load scenario can be attained using the following equations [49]:

$$\tau_{d,i} = \int_{P_{d,i}^{min}}^{P_{d,i}^{max}} \frac{1}{\sigma_d\sqrt{2\pi}} exp\left[-\frac{(P_d - \mu_d)^2}{2\sigma_d^2}\right] dP_d \tag{26}$$

$$P_{d,i} = \frac{1}{\tau_{d,i}} \int_{P_{d,i}^{min}}^{P_{d,i}^{max}} \frac{P_d}{\sigma_d\sqrt{2\pi}} exp\left[-\frac{(P_d - \mu_d)^2}{2\sigma_d^2}\right] dP_d \tag{27}$$

where, $P_{d,i}^{min}, P_{d,i}^{max}$ represent the border limits of interval i.

D. LOAD GENERATION MODEL

Combining load scenarios, wind speed, and irradiation model probabilities can be attained by multiplying their probabilities in (21), (24), and (26) as:

$$\tau_s = \tau_{d,i} \times \tau_{solar,m} \times \tau_{wind,k} \tag{28}$$

E. BACKWARD REDUCTION ALGORITHM

Using the backward reduction algorithm (BRA) in scenario reduction steps are illustrated in [34]. Table 1 lists the designated demonstrative scenarios with their corresponding probabilities. Each row in this table provides data for each scenario including the percentage of loading, wind speed, solar irradiance, wind power, PV power, and the probability for the scenario.

TABLE 1. Designated scenarios and corresponding parameters for studied scenarios.

Scenario no.	% Loading *Pd*	Wind speed v_w(m/s)	Irradiance, G_s (W/m^2)	Wind power (MW)	PV power (MW)	Scenario probability, Δ_{sc}
1	60.293	6.514	918.376	20.272	45.919	0.001
2	76.831	13.347	1924.466	59.697	50.000	0.001
3	69.559	11.289	1340.112	47.819	50.000	0.001
4	77.134	15.633	655.062	72.882	32.753	0.003
5	49.093	20.535	179.330	75.000	8.967	0.001
6	65.263	8.282	784.890	30.473	39.245	0.001
7	67.261	9.530	205.853	37.673	10.293	0.119
8	92.929	11.278	343.400	47.757	17.170	0.001
9	42.659	4.289	0.000	7.439	0.000	0.007
10	72.131	5.227	0.000	12.845	0.000	0.489
11	68.524	11.584	614.511	49.523	30.726	0.008
12	66.030	2.439	568.783	0.000	28.439	0.009
13	66.065	8.047	718.424	29.118	35.921	0.002
14	67.521	7.052	1435.959	23.378	50.000	0.001
15	61.892	9.308	57.991	36.394	1.401	0.003
16	74.331	8.387	166.863	31.077	8.343	0.119
17	68.012	7.955	280.474	28.586	14.024	0.090
18	59.917	6.432	435.519	19.798	21.776	0.017
19	72.927	6.206	748.389	18.497	37.419	0.001
20	66.075	7.357	529.017	25.136	26.451	0.007
21	65.005	11.852	327.512	51.068	16.376	0.045
22	62.978	11.275	485.290	47.738	24.265	0.014
23	72.318	8.387	382.131	31.078	19.107	0.028
24	98.525	0.617	180.523	0.000	9.026	0.003
25	79.921	5.220	93.790	12.810	3.665	0.029

IV. OVERVIEW OF RAO-3

Rao is a recently developed optimization algorithm [55]. There are three proposed Rao algorithms namely Rao-1, Rao-2, and Rao-3. It's selected for use in this research as a population-based algorithm due to its simplicity, ease of implementation in optimization applications. Moreover, it has fewer control parameters as it has not a metaphorical explanation. The swarm size is the only control parameter that needs adjustment once the stop condition is attained. Like iterative optimization algorithms, Rao algorithms explore the search space to get iteration finest solution, iteration worst solution, and arbitrary exchanges among the swarm. In [55], the performance Rao method has been validated using 23 benchmark functions, 25 unconstrained benchmark functions and 2 standard constrained optimization problems. The experimental results have been shown that the RAO algorithm can guarantee the performance of explorations while achieving superior exploitations, thus maintaining an outstanding balance between exploitations and explorations, which reflects the superior performance of the algorithm in a statistical sense compared with other algorithms. Roa method has been used for solving several engineering optimization problems [56]–[61].

The three algorithms of Rao are similar in their steps but they only differ in the movement equation as illustrated in the following steps and depicted in Figure 4 [60]:

1. Express population size N_{pop}, the dimension of optimization variables, *dim*, Minimum and Maximum limits of variables, Var^{min}, Var^{max} and the predetermined stop criteria.

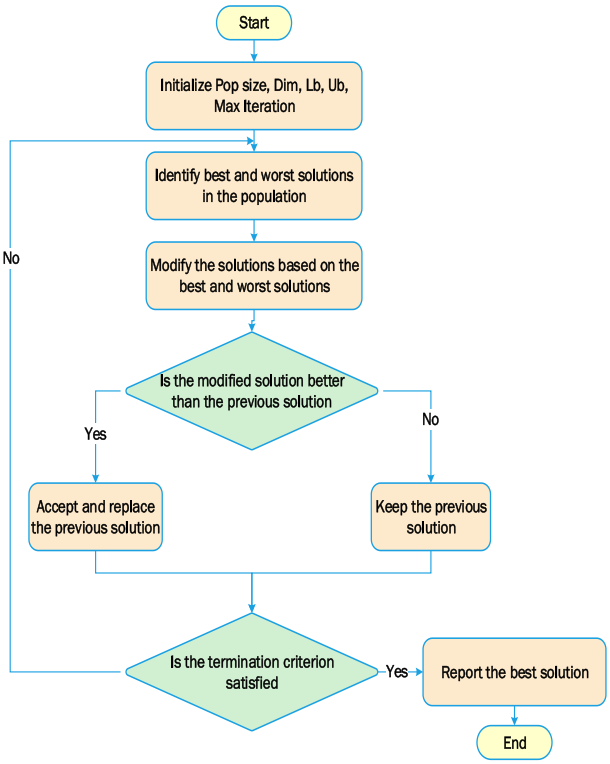

FIGURE 4. Flowchart for implementation of Rao-3 algorithm.

2. Random initialization of population and corresponding fitness function evaluation.
3. Extract the best and worst solutions from the populations based on their objective function values.

4. Update the new solution for all population $p = 1, 2, \ldots, N_{pop}$, in the current k^{th} iteration which depends on the selected Rao- algorithm as follows:
   a) *Rao-1 Algorithm,* the following equation is used to find the updated solution x':
   $$x'_{m,p,k} = x_{m,p,k} + r_{1,m,k}\left(x_{m,q,k} - x_{m,w,k}\right) \quad (29)$$
   where, $x_{m,p,k}$ is m^{th} variable value for the p^{th} solution during the i^{th} iteration. The best candidate solution is denoted by $x_{m,q,k}$ while $x_{m,w,k}$ is the value of the worst solution.
   b) *The Rao-2 algorithm,* the following equation is used to obtain the updated solution:
   $$x'_{m,p,k} = x_{m,p,k} + r_{1,m,k}\left(x_{m,q,k} - x_{m,w,k}\right) + r_{2,m,k} \times \left(\left|x_{m,p,k} \text{ or } x_{m,d,k}\right| - \left|x_{m,d,k} \text{ or } x_{m,p,k}\right|\right) \quad (30)$$
   where $r_{1,m,k}$, $r_{2,m,k}$ are random numbers in the range of [0, 1] for the m^{th} variable value in i^{th} iteration. The additional term in (30) represents the random interaction through the population.
   c) *Rao-3 algorithm,* the following equation is used to obtain the updated solution:
   $$x'_{m,p,k} = x_{m,p,k} + r_{1,m,k}\left(x_{m,q,k} - \left|x_{m,w,k}\right|\right) + r_{2,m,k}\left(\left|x_{m,p,k} \text{ or } x_{m,d,k}\right| - \left(x_{m,d,k} \text{ or } x_{m,p,k}\right)\right) \quad (31)$$
5. In this phase, the cost function is evaluated according to the updated population. The objective function values are sorted to get the best solution to be compared with the old solution. If the new solution is better than its old value, then the old value will be updated by the new one.
6. Finally, the termination criterion will be investigated. If this condition isn't attained, go to Step 3 else print the optimal solution of the optimization problem.

V. SIMULATION RESULTS AND DISCUSSION

In the present work, the standard configurations of the IEEE 30-bus, IEEE 57-bus systems, and IEEE 118-bus are considered for the implementation of selected cases of deterministic ORPD. Moreover, comparing the results of those cases using the proposed Rao-3 algorithm with recent results concluded. All generators in standard configurations are thermal generators. While a modification to the IEEE 30- bus system by replacing the thermal generator at bus 5 with wind power generating source and the thermal generator at bus 8 with a photovoltaic (PV) power unit is considered. Optimal locations of the wind farm and PV power generation depend on several factors such as wind speed and solar radiation, respectively [58]. In this paper, the locations of wind and PV units are selected as in [34], with the aim of comparing the obtained results with those mentioned in [34].

This will lead to executing stochastic ORPD including a wind generator and a PV unit. Figure 5 shows a diagram of the modified system.

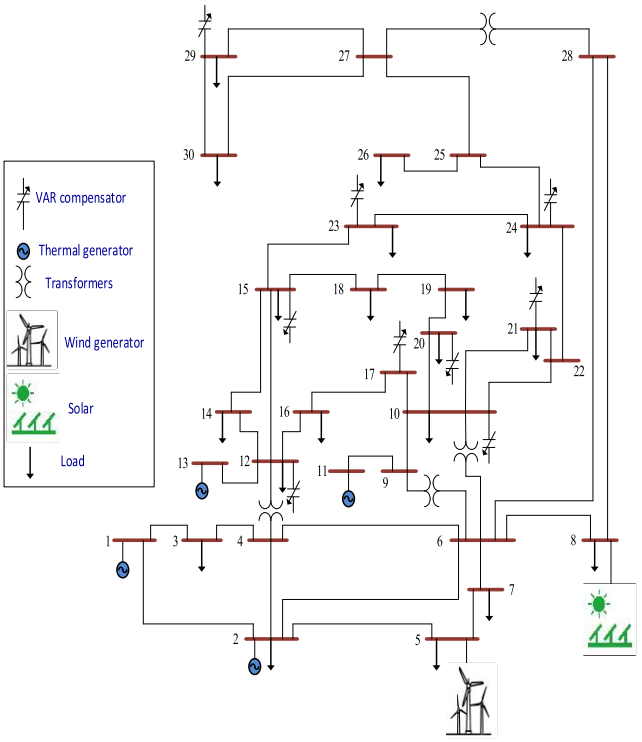

FIGURE 5. The customized IEEE 30-bus system with wind power generator and PV power unit.

This section investigates the capability of the Rao-3 optimization algorithm to solve the ORPD problem with and without considering the uncertainty of renewable energy resources [62]. IEEE 30-bus, 57-bus, and 118-bus are considered as test systems. Two recent optimization techniques, Artificial electric field algorithm (AEFA) [63], and artificial Jellyfish Search (JS) [64] algorithms as well as other well-known algorithms are used to validate the proposed algorithm to solve the ORPD problems. Table.11 in the appendix summarizes the details of studied cases; configuration, variables number, and limits. Generators data for the IEEE 30-bus and IEEE 57-bus systems are given in the Appendix, Table 9, and Table 10. The limit setting for control variables of the IEEE 118-bus system is presented in Table 12 in the Appendix. The proposed Rao based ORPD is executed via MATLAB 2016a platform using an Intel ® core TM i5-7200U CPU, 2.50 GHz, 8 GB RAM Laptop. Test system-1: IEEE 30-bus test system (Base-case).

A. TEST SYSTEM-1 (BASE CASE): IEEE 30-BUS SYSTEM

Case (1) will handle the minimization of real power loss (P_{loss}) while Case (2) will investigate the minimization of cumulative voltage deviation (VD) of PQ buses for the standard configuration of the IEEE 30-bus system. These two cases consider more realistic mixed-integer optimization problems where the capacitor banks and transformer taps are treated as discrete variables. The capacitor can be switched in discrete steps of 0.2 MVAr and transformer tap settings can be changed in steps of 0.02 p.u. from 0.90 to1.10 p.u.

TABLE 2. Results of studied cases for 30-bus system.

Parameters	Min	Max	Case 1(Min. P_{loss})			Case 1a(Min. P_{loss})			Case 2(Min. VD)			Case 2a (Min. VD)		
			JS	AEFA	Rao-3	JS	AEFA	Rao-3	JS	AEFA	Rao-3	JS	AEFA	Rao-3
Generator voltage														
V1 (p.u.)	0.95	1.1	1.0647	1.0652	1.0693	1.0709	1.0716	1.0718	1.0085	1.0091	1.0030	1.0105	1.0130	1.0026
V2 (p.u.)	0.95	1.1	1.0566	1.0570	1.0609	1.0616	1.0616	1.0626	1.0072	1.0074	0.9999	1.0075	1.0110	0.9981
V5 (p.u.)	0.95	1.1	1.0333	1.0335	1.0373	1.0392	1.0372	1.0405	1.0202	1.0225	1.0180	1.0230	1.0202	1.0162
V8 (p.u.)	0.95	1.1	1.0392	1.0394	1.0433	1.0398	1.0376	1.0407	1.0064	1.0049	1.0079	1.0036	1.0057	1.0084
V11 (p.u.)	0.95	1.1	1.0754	1.0915	1.0821	1.0749	1.0818	1.0906	1.0277	1.0306	1.0425	1.0026	1.0368	1.0742
V13 (p.u.)	0.95	1.1	1.0690	1.0737	1.0469	1.0593	1.0672	1.0517	1.0083	1.0359	1.0145	1.0360	1.0289	1.0151
Transformer tap ratio														
T11 (p.u.)	0.9	1.1	1.0089	1.0388	1.1	1.0139	1.0132	1.0756	1.0229	0.9771	1.0618	1.0135	1.0271	1.1000
T12 (p.u.)	0.9	1.1	1.0049	0.9199	0.9004	0.9696	0.9178	0.9008	0.9217	0.9151	0.9000	0.9024	0.9000	0.9000
T15 (p.u.)	0.9	1.1	1.0248	1.0220	0.9763	0.9989	1.0003	0.9883	0.9703	0.9942	0.9964	1.0230	0.9885	0.9980
T36 (p.u.)	0.9	1.1	0.9822	0.9604	0.9809	0.9743	0.9611	0.9751	0.9660	0.9567	0.9510	0.9630	0.9661	0.9696
Capacitor bank														
QC10 (MVAr)	0	5	4.9294	2.9937	4.6402	4.5288	2.5307	0.0000	4.8648	1.0064	4.9928	4.9997	3.4076	4.9998
QC12 (MVAr)	0	5	4.2358	2.4933	3.2615	3.0668	2.2560	3.6542	2.3527	2.1341	5.0000	0.0229	2.4756	4.9858
QC15 (MVAr)	0	5	4.7241	2.7821	3.9266	3.7421	1.5519	4.2518	4.9099	0.6094	4.9992	4.9999	1.7885	5.0000
QC17 (MVAr)	0	5	4.9272	2.6618	5	4.9854	2.3641	5.0000	0.0455	2.2762	0.0786	0.0052	1.6987	0.0011
QC20 (MVAr)	0	5	2.5270	2.4448	3.9943	3.9833	3.0356	3.9864	4.9659	2.6099	4.9123	4.9997	1.8460	4.9997
QC21 (MVAr)	0	5	4.9503	3.9928	5	4.9996	3.3146	4.9999	4.8045	1.6892	4.9859	4.9930	4.1092	4.9999
QC23 (MVAr)	0	5	3.0033	3.1462	2.9479	2.9786	1.3546	2.8600	4.9103	3.6124	4.9813	4.9999	3.6816	5.0000
QC24 (MVAr)	0	5	4.9555	0.7065	5	4.9980	1.7375	4.9980	4.9020	2.9580	4.9998	5.0000	1.6443	4.9999
QC29 (MVAr)	0	5	2.3300	1.4672	2.5716	2.3982	1.9316	2.4654	2.0288	3.4338	1.8802	2.4052	4.2120	2.6200
Objective function														
Ploss (MW)	NA	NA	4.4289	4.4711	**4.4124**	4.8635	4.9393	**4.8612**	5.3390	5.3886	5.4632	5.8489	5.7490	6.0307
VD (p.u.)	NA	NA	0.8564	0.8839	0.8840	0.9207	0.8938	0.9205	0.0947	0.1418	**0.0883**	0.0944	0.1313	**0.0873**
Generator reactive power														
QG1 (MVAr)	-20	150	-3.599	-3.101	-0.530	-0.499	2.3175	0.0488	-19.99	-20.000	-20.00	-19.963	-20.000	-19.998
QG2 (MVAr)	-20	60	12.427	13.111	16.114	15.498	18.279	15.949	1.2864	-0.1970	-13.896	-4.041	4.0171	-19.909
QG5 (MVAr)	-15	62.5	24.721	24.929	24.702	24.336	24.144	24.619	58.536	61.717	59.281	58.468	52.582	53.685
QG8 (MVAr)	-15	48.7	26.529	28.983	28.789	30.616	35.140	29.937	48.700	48.700	48.700	48.694	48.700	48.681
QG11 (MVAr)	-10	40	13.706	24.840	28.105	14.194	16.897	28.210	11.704	7.3723	21.920	1.6546	15.357	38.727
QG13 (MVAr)	-15	44.7	15.083	18.767	-1.685	7.3226	13.348	1.5319	0.1252	16.445	4.7783	20.115	11.335	4.8920

The optimization technique performs a rounding operation in order to handle these discrete variables [34].

As the generators' active power settings (except the swing generator) are necessary for the ORPD, the values of the active power are carefully selected around the generators' specified limits. The values of the active power of generators are listed in Table 9 in the Appendix. Besides cases 1 and 2, the other two cases Case (1a) and Case (2a) are investigated with the same aim of minimizing P_{loss} and the total VD, respectively.

These cases consider the setting values of the active power of generators which are presented in [65], and also listed in Table 9.

Table 2 provides all the control variables' settings and their permissible limits to study the objective function of 4 cases (i.e. Case (1), Case (2), Case (1a), and Case (2a)) related to the IEEE 30-bus system. The negative values of reactive power imply the absorption of reactive power by the generator. Figure 6 shows the voltage profile of PQ buses for the four study cases.

In Case (1) and Case (1a), voltage values of a few PQ buses increased and became close to the maximum limit to achieve minimum power loss. While in Case (2) and Case (2a) of reducing the cumulative VD shall not drive to an increase of voltage because the main objective in these cases is to keep the buses voltage nearby 1.0 p.u.

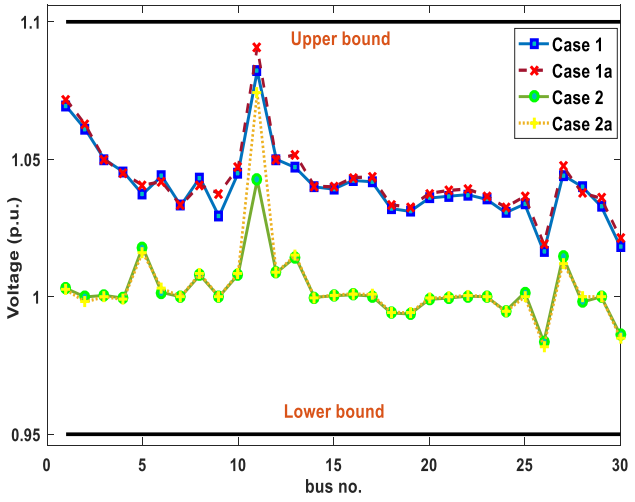

FIGURE 6. PQ buses Voltage profiles for the investigated cases of IEEE 30-bus test system.

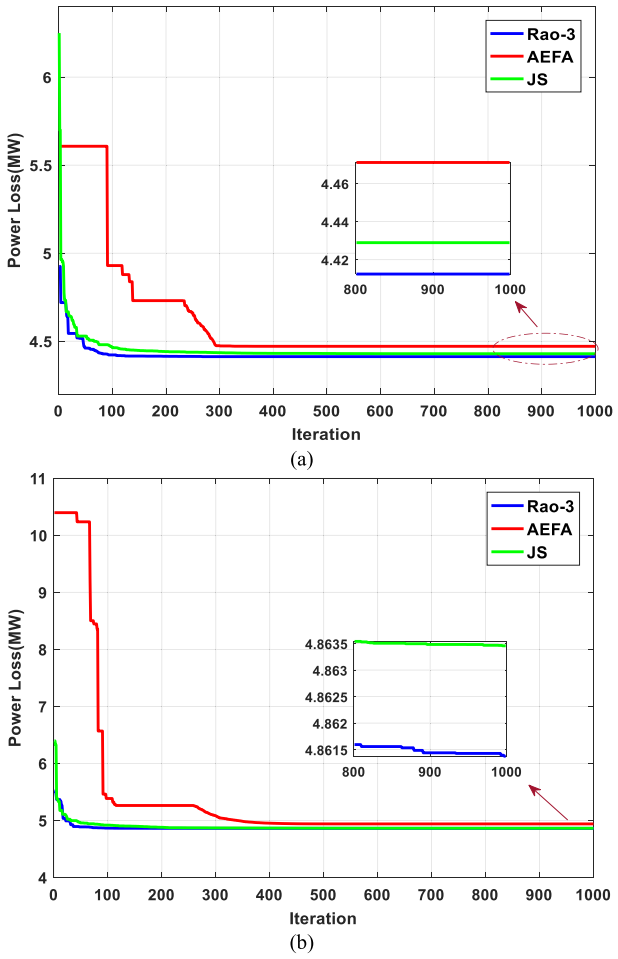

FIGURE 7. The convergence characteristics of the proposed Rao-3, AEFA, and JS algorithms for studied cases of power losses for the IEEE 30-bus system (a) Case 1 (b) Case 1a.

The convergence characteristics of the Rao-3, AEFA, and JS algorithms for the Case (1) & Case (1a), and Case (2) & Case (2a) are shown in Figure 7 and Figure 8, respectively.

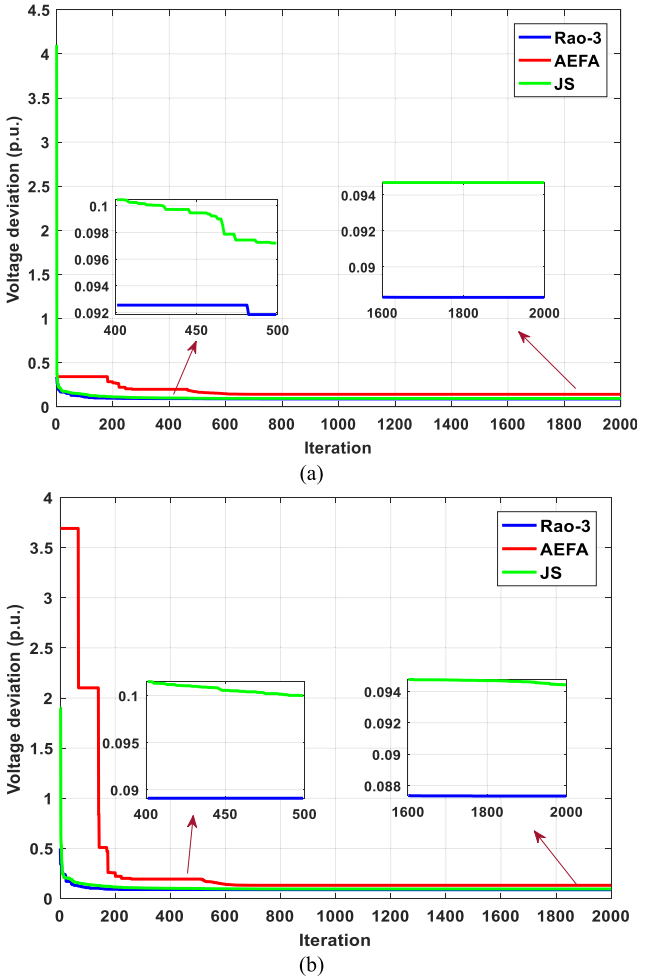

FIGURE 8. The convergence characteristics of the proposed Rao-3, AEFA, and JS algorithms for studied cases of voltage deviations minimization for IEEE 30-bus system (a) Case 2 (b) Case 2a.

In Figures 7 and 8, the focus has been made on the proposed Rao-3 and JS algorithms, because the results of AEFA is the worst in these cases. The least power losses obtained by the proposed algorithm in Cases (1) and Case (1a) are 4.4124 MW and 4.8612 MW, respectively, although the optimal value of *VD* in Case (2) and Case (2a) are 0.08830 p.u. and 0.0873 p.u, respectively.

Table 3 shows a comparison of the results obtained by the proposed algorithm in the current study with certain previously published ORPD results. There are few references in the table which specifically address the active power settings of the specific generators. All these references are presumed to have tracked the given data in [65].

The proposed algorithm achieves the optimum solution in Case 1 (4.4124 MW) compared with the two recent AEFA and JS algorithms and the other published algorithms as shown in Table 3. The detailed analyses of infeasible solutions using some algorithms in Table 3 are mentioned in [34]. In a comparison of Case (2) and Case (2a), the results of previous papers using several algorithms reached relatively

TABLE 3. Results comparison of investigated cases for IEEE 30-bus system.

Case no.	Algorithm	Power loss P_{loss} (MW)	Voltage dev. VD (p.u.)
Case 1	Rao-3	4.4124	0.8840
	AEFA	4.4711	0.8839
	JS	4.4289	0.8564
	SHADE-EC [34]	4.4126	0.9029
Case 1a	Rao-3	4.8612	0.9205
	AEFA	4.9393	0.8938
	JS	4.8635	0.9207
	SHADE-EC [34]	4.8612	0.9205
	DE [66]	4.5550	1.9589[b]
	QOTLBO [27]	4.5594	1.9057[b]
	MFO [67]	4.5128	-
	EMA [65]	4.4978	0.8123
	IGSA-CSS [68]	4.7660[a]	-
	OGSA [69]	4.4984	0.8085
	HFA [70]	4.529	1.625[b]
	FAHCLPSO [71]	4.4877	-
	NGBWCA [30]	4.4801	0.8413
Case 2	Rao-3	5.4632	0.08830
	AEFA	5.3886	0.1418
	JS	5.3390	0.0947
	SHADE-EC [34]	5.4495	0.08886
Case 2a	Rao-3	6.0307	0.0873
	AEFA	5.7490	0.1313
	JS	5.8489	0.0944
	SHADE-EC [34]	6.0099	0.08724
	QOTLBO [27]	6.4962	0.0856
	MFO [67]	-	0.12154
	EMA [65]	6.241	0.06131
	IGSA-CSS [68]	-	0.08968[a]
	OGSA [69]	6.9044	0.0640
	HFA [70]	5.75	0.0980
	FAHCLPSO [71]	-	0.04315
	NGBWCA [30]	6.3142	0.0458

[a] *Higher limit for PQ buses voltage and generator reactive power are utilized*
[b] *Infeasible approach, bus voltage load restriction is violated*

lower values of VD, but no publication listed here checked the actual reactive power generation status or the PQ-bus voltage profile [34].

B. TEST SYSTEM-2 (BASE CASE): IEEE 57-BUS SYSTEM

Minimizing P_{loss} and cumulative VD for the IEEE 57-bus system have been studied in Case (3) and Case (4). The setting values of the generators' active power for the IEEE 57-bus system have been listed in Table 10.

In Case (3) and Case (4), the active power of thermal units' isn't adjusted to zero. Three thermal units are selected with zero active power in Case (3a) and (4a). Hence, they are either absorbing or producing reactive power.

Like the IEEE 30-bus system, Table 4 provides the settings of all control variables and their permissible limits to study the objective function of the four cases (i.e. Case (3), Case (4), Case (3a), and Case (4a)) related to the IEEE 57-bus system. Figure 9 shows the voltage profile of PQ buses for the four cases of the IEEE 57-bus system. The convergence characteristics of the Rao-3, AEFA, and JS algorithms are displayed in Figure 10 for Case (3) and Case (3a) while Figure 11 shows the convergence characteristics of the proposed Rao-3, AEFA, and JS for Case (4) and Case (4a). Because the results of the JS technique are the nearest to those obtained by the Rao-3, the focus in the convergence curves has been made on both of them. All convergence curves of Figures 10 and 11 prove that the Rao-3 gives the best solutions for the ORPD problem.

Table. 5 presents the results IEEE of the 57-bus system obtained by the developed algorithm compared with those obtained by other well-known optimization techniques. The developed algorithm achieves the optimal solution in Case (3) with 18.1494 MW compared with the solution obtained by the SHADE-EC algorithm (18.4000 MW). While the SHADE-EC and the Rao-3 achieve the best solutions in Case (3a) among the results of all algorithms listed in Table.7, these solutions are 23.3031 MW and 23.3040 MW, respectively. The Rao-3 algorithm achieves also the optimal solution (0.6160 p.u.) in Case (4) compared with the SHADE-EC algorithm (0.62632 p.u.) while the SHADE-EC and Rao-3 achieve the best result in Case (3a) among the

TABLE 4. Numerical results of studied cases for IEEE57-bus system.

Parameters	Min	Max	Case 3(Min. P_{loss})			Case 3a(Min. P_{loss})			Case 4(Min. VD)			Case 4a (Min. VD)		
			JS	AEFA	Rao-3	JS	AEFA	Rao-3	JS	AEFA	Rao-3	JS	AEFA	Rao-3
Generator voltage														
V1 (p.u.)	0.95	1.1	1.0810	1.0533	1.0951	1.0837	1.0466	1.0883	1.0187	1.0512	1.0152	1.0107	1.0468	1.0209
V2 (p.u.)	0.95	1.1	1.0733	1.0426	1.0874	1.0732	1.0318	1.0774	1.0168	1.0372	1.0119	0.9968	1.0327	1.0116
V3 (p.u.)	0.95	1.1	1.0581	1.0189	1.0716	1.0624	1.0095	1.0652	1.0212	1.0146	1.0125	1.0075	1.0126	1.0102
V6 (p.u.)	0.95	1.1	1.0584	0.9932	1.0626	1.0559	0.9907	1.0559	1.0129	0.9798	1.0027	1.0126	0.9876	1.0043
V8 (p.u.)	0.95	1.1	1.0723	0.9970	1.0771	1.0746	1.0012	1.0752	1.0262	0.9578	1.0166	1.0492	0.9751	1.0309
V9 (p.u.)	0.95	1.1	1.0459	0.9811	1.0522	1.0448	0.9776	1.0427	1.0068	0.9617	1.0020	1.0169	0.9681	1.0072
V12 (p.u.)	0.95	1.1	1.0484	0.9982	1.0556	1.0521	0.9944	1.0442	1.0271	1.0095	1.0316	1.0326	1.0178	1.0345
Transformer tap ratio														
T19 (p.u.)	0.9	1.1	1.0110	1.0261	0.9000	1.0186	0.9704	0.9953	0.9964	1.0345	0.9130	0.9489	0.9529	1.0945
T20 (p.u.)	0.9	1.1	0.9904	0.9262	1.0534	0.9786	0.9289	0.9904	1.0215	0.9453	1.0239	1.0090	1.0418	0.9024
T31 (p.u.)	0.9	1.1	1.0021	1.0244	1.0132	1.0040	1.0016	1.0032	0.9868	0.9813	0.9738	0.9723	0.9732	0.9729
T35 (p.u.)	0.9	1.1	1.0492	1.0069	0.9871	1.0287	1.0508	1.0589	0.9738	0.9613	1.0979	1.0005	0.9626	1.0494
T36 (p.u.)	0.9	1.1	1.0277	1.0675	1.0802	0.9961	1.0043	0.9675	0.9533	1.0764	0.9931	1.0990	1.0625	1.0956
T37 (p.u.)	0.9	1.1	1.0201	1.0202	1.0250	1.0028	1.0118	1.0061	1.0278	1.0418	1.0219	1.0418	1.0030	1.0075
T41 (p.u.)	0.9	1.1	1.0258	0.9242	1.0098	0.9969	0.9330	0.9967	0.9877	0.9207	0.9894	0.9924	0.9503	1.0001
T46 (p.u.)	0.9	1.1	0.9591	0.9474	0.9658	0.9533	0.9518	0.9541	0.9767	0.9421	0.9165	0.9185	0.9302	0.9175
T54 (p.u.)	0.9	1.1	1.0028	0.9406	0.9000	0.9103	0.9430	0.9083	0.9056	0.9098	0.9002	0.9000	0.9000	0.9000
T58 (p.u.)	0.9	1.1	0.9898	0.9557	0.9936	0.9884	0.9379	0.9899	0.9596	1.0003	0.9328	0.9746	0.9667	0.9305
T59 (p.u.)	0.9	1.1	0.9891	0.9419	0.9797	0.9723	0.9168	0.9685	0.9791	0.9202	0.9869	0.9562	0.9162	0.9882
T65 (p.u.)	0.9	1.1	0.9923	0.9394	0.9854	0.9813	0.9157	0.9729	1.0083	0.9618	1.0075	1.0070	0.9871	1.0011
T66 (p.u.)	0.9	1.1	0.9686	0.9236	0.9491	0.9450	0.9000	0.9402	0.9041	0.9026	0.9055	0.9000	0.9000	0.9000
T71 (p.u.)	0.9	1.1	0.9535	0.9187	0.9919	0.9728	0.9033	0.9705	0.9449	0.9216	0.9482	0.9535	0.9287	0.9598
T73 (p.u.)	0.9	1.1	1.0213	0.9784	0.9755	0.9874	0.9943	0.9921	1.0161	0.9755	1.0415	1.0339	0.9668	1.0049
T76 (p.u.)	0.9	1.1	0.9849	0.9052	0.9601	0.9596	0.9825	0.9582	0.9406	0.9427	0.9002	0.9009	0.9166	0.9008
T80 (p.u.)	0.9	1.1	1.0225	0.9405	0.9980	0.9869	0.9204	0.9857	0.9987	0.9586	1.0073	1.0170	0.9257	0.9895
Capacitor bank														
QC18 (MVAr)	0	20	10.569	8.3834	0.0908	9.9950	9.5114	7.5083	14.382	6.4584	3.5534	0.4752	9.0094	0.0177
QC25 (MVAr)	0	20	16.691	17.894	15.533	14.904	14.414	14.585	14.081	15.205	16.306	14.8260	15.744	19.9031
QC53 (MVAr)	0	20	14.369	4.8200	13.385	13.122	18.227	13.085	19.049	19.093	19.998	19.9967	4.8656	19.9693
Objective function														
Ploss (MW)	NA	NA	18.594	20.610	**18.149**	23.356	25.648	**23.304**	21.361	22.841	21.973	28.4017	27.639	27.5977
VD (p.u.)	NA	NA	1.2894	1.0288	1.7845	1.7323	1.3024	1.7397	0.7050	0.8377	**0.6160**	0.6443	0.7747	**0.5993**
Generator reactive power														
QG1 (MVAr)	-140	200	54.376	96.461	60.995	40.413	88.285	55.475	-18.17	100.27	-16.001	-7.4453	67.127	-9.0039
QG2 (MVAr)	-17	50	49.999	50	49.986	50.000	50.000	49.986	49.999	36.695	49.553	17.5333	50.000	47.1818
QG3 (MVAr)	-10	60	21.258	41.136	39.278	41.816	39.466	47.891	59.991	47.067	59.801	59.9602	48.721	59.9360
QG6 (MVAr)	-8	25	-2.551	-3.724	-6.279	-0.111	1.8748	-2.204	-7.985	16.615	-7.4606	-5.1635	24.999	-5.5818
QG8 (MVAr)	-140	200	56.529	28.126	55.355	63.394	37.199	70.002	40.872	-41.293	29.808	90.5450	-18.272	54.2915
QG9 (MVAr)	-3	9	54.376	9	8.9829	9.0000	9.0000	8.9304	8.9984	6.4983	8.9146	8.7947	8.9999	8.6487
QG12 (MVAr)	-150	155	49.999	56.214	51.789	65.125	61.521	42.827	130.34	114.77	154.26	145.2297	131.15	149.912 8

results of all algorithms by 0.59673 p.u.and 0.5993 p.u., respectively.

C. TEST SYSTEM-3: MODIFIED IEEE 30-BUS TEST SYSTEM

In this subsection, the modified IEEE 30-bus system is studied. In the modified test system, the thermal generator at bus #5 is substituted by a wind turbine generator while the thermal generator at bus #8 is replaced with a PV unit. The load demand, wind turbine generated power, and PV power is variable based on diverse scenarios as explained previously. Shunt reactive power compensators and transformer tapping settings are discrete steps as in Case (1) and Case (2). Table 9 in the appendix provides the active power thermal generator settings values (except swing generator). Hence, the swing bus must be able for achieving the balance of real power whenever there is a shortage in the supply from these renewable energy sources. The ultimate value of the active output power of the swing generator is considered high enough (200 MW) in this research which satisfies load needs even if the active power output from the RES is zero.

The range of the wind power generator and the PV unit VAR is assumed almost in the range of $[-0.4, 0.5]$ p.u. within their range of real output power. An explanation for this assumption is given in [46]. Table 9 in the appendix lists these values of reactive power. The two objectives (P_{loss} & VD) of the ORPD problem are minimized as single objectives, and then, jointly, as a multi-objective function.

D. SINGLE OBJECTIVE STOCHASTIC ORPD

The stochastic ORPD with uncertain wind power has been proposed in [49], [74] where the detailed information about stochastic ORPD has been presented in [34]. The minimization of expected power loss (EPL) in Case (5) needs an optimization algorithm to run 25 times for 25 scenarios.

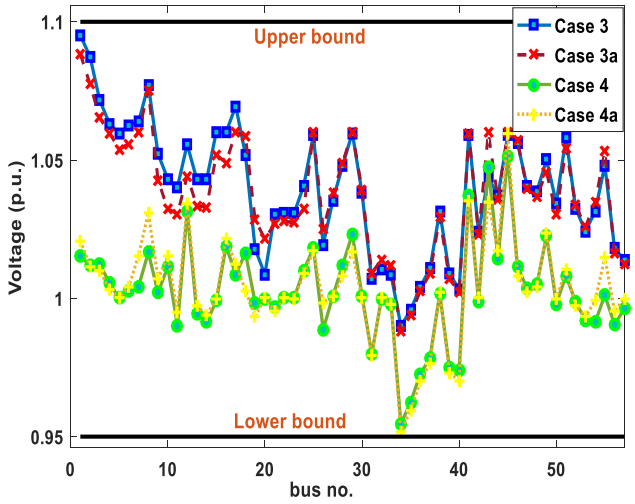

FIGURE 9. Voltage profiles of PQ buses for the studied cases of 57-bus system.

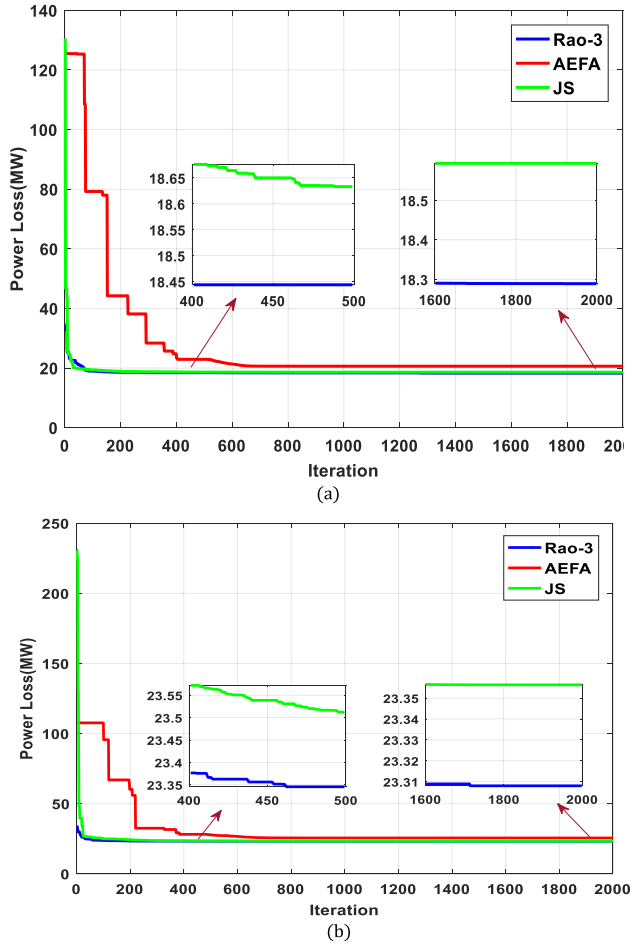

FIGURE 10. The convergence curves of the proposed Rao-3, AEFA, and JS algorithms for studied cases of P_{loss} for 57-bus system (a) Case 3 (b) Case 3a.

For each scenario, Table 6 provides the minimized value of power loss (P_{loss}). Defining the scenario probability as Δ_{SC} and minimized power loss is P_{loss}, the estimated power

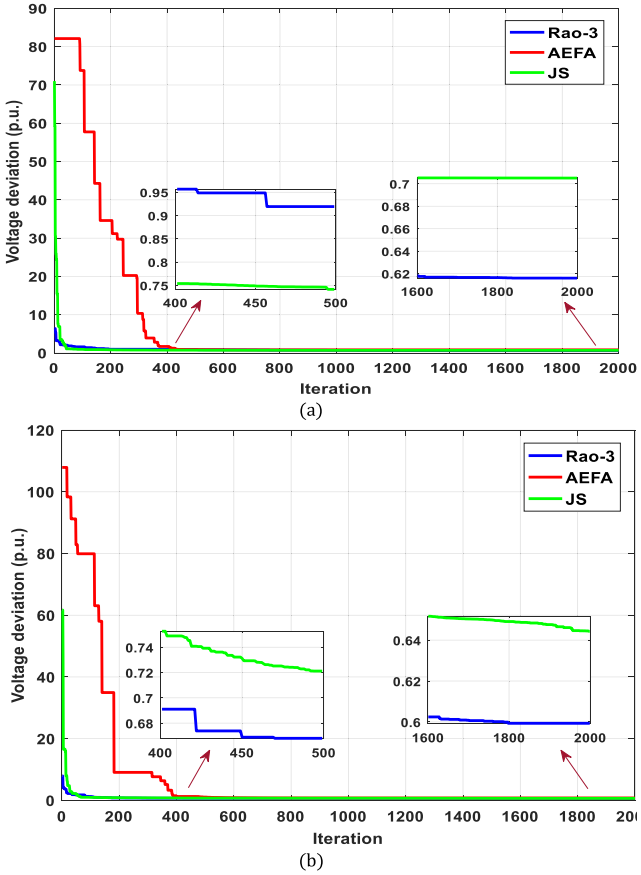

FIGURE 11. The convergence curves of the proposed Rao-3, AEFA, and JS algorithms for studied cases of VD for IEEE 57-bus system (a) Case (4) (b) Case (4a).

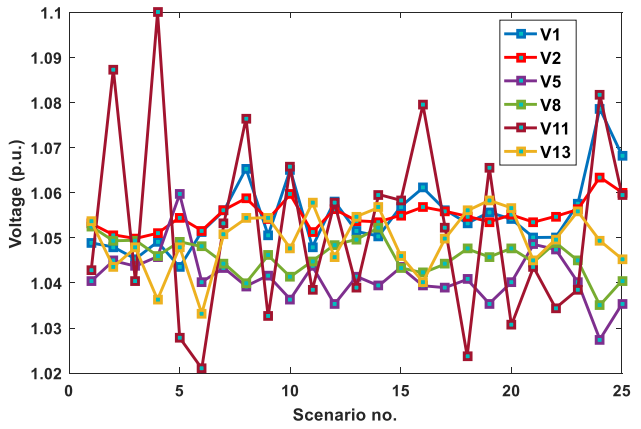

FIGURE 12. Optimum values of PV bus voltages for studied scenarios in Case 5.

loss (EPL) is evaluated for all scenarios as follows:

$$EPL = \sum_{sc=1}^{Nsc} \Delta_{sc} X P_{loss,sc} \tag{32}$$

where, N_{SC} denotes the total number of evaluated scenarios. Similarly, VD for every scenario is minimized in Case 6.

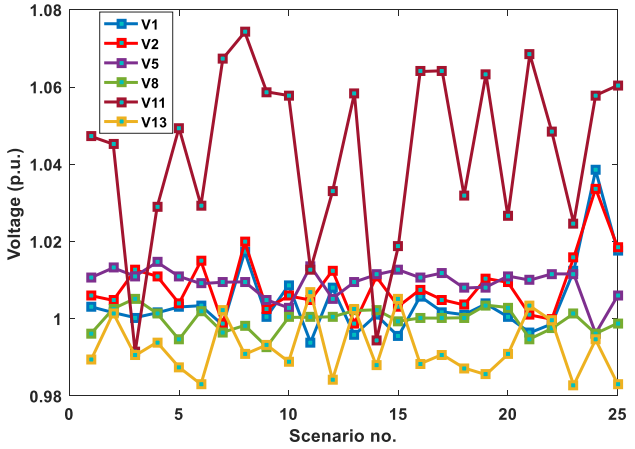

FIGURE 13. Optimal values of PV bus voltages for studied scenarios in Case 6.

TABLE 5. Results comparison of evaluated cases for the IEEE 57-bus system.

Case no.	Algorithm	Power loss P_{loss} (MW)	Voltage dev. VD (p.u.)
Case 3	Rao-3	18.1494	1.7845
	AEFA	20.610	1.0288
	JS	18.594	1.2894
	SHADE-EC [34]	18.4000	1.5207
Case 3a	Rao-3	23.3040	1.7397
	AEFA	25.648	1.3024
	JS	23.356	1.7323
	SHADE-EC [34]	23.3031	1.7322
	MFO [67]	24.2529	-
	IGSA-CSS [68]	22.2718[a]	-
	OGSA [69]	23.43	1.1907
	ICA [72]	24.1607	-
	PSO-ICA [72]	24.1386	-
	MICA-IWO [73]	24.2568	-
Case 4	Rao-3	21.9733	0.6160
	AEFA	22.841	0.8377
	JS	21.361	0.7050
	SHADE-EC [34]	21.6013	0.62632
Case 4a	Rao-3	27.5977	0.5993
	AEFA	27.639	0.7747
	JS	28.4017	0.6443
	SHADE-EC [34]	27.7317	0.59673
	IGSA-CSS [69]	-	0.60347[a]
	OGSA [69]	32.34	0.6982
	ICA [72]	-	0.6137
	PSO-ICA [72]	-	0.6031

[a] *Different limits of generator reactive power are utilized*

Table 7 presents the optimized values of VD_{sc} for all scenarios. The expected voltage deviation (EVD) over all scenarios is expressed as:

$$EVD = \sum_{sc=1}^{Nsc} \Delta_{sc} X VD_{sc} \tag{33}$$

The value of EPL obtained for Case (5) is 2.4998 MW and EVD for Case (6) is 0.06314 p.u. In Table 6, the power loss is the lowest value when system loading is at its minimum level (scenario 9, loading = 42.659%). Minimum loading implies the lowest current in the network and hence low power loss.

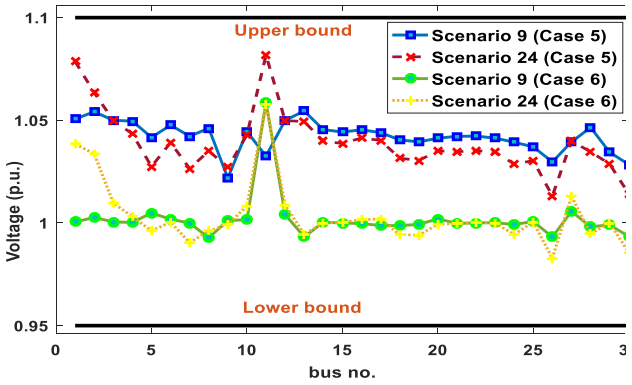

FIGURE 14. Voltage profiles of Load bus for the extreme scenarios in Cases 5 and 6.

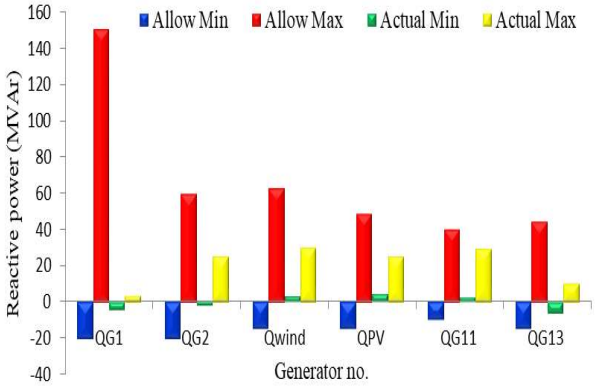

FIGURE 15. Upper and lower reactive power values of the generators for all scenarios in Case 5.

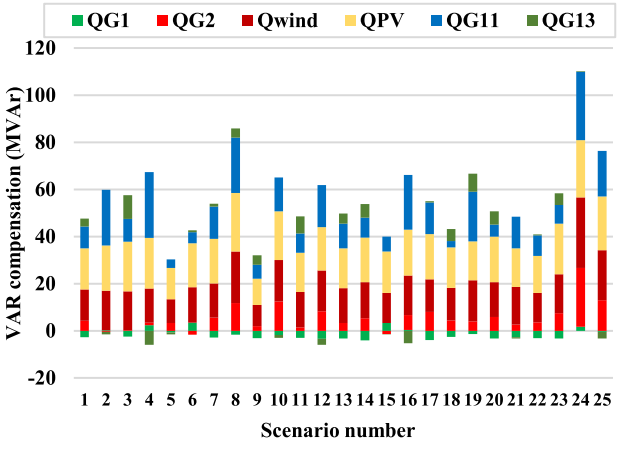

FIGURE 16. Reactive power values of the generators for all scenarios of Case 5.

In the contrast, the highest value of the power loss is achieved when the system loading is at its maximum level with the absence of wind power (scenario 24, loading = 98.525%, wind power = 0 MW). Because of the lack of wind power, the swing generator has to supply surplus power to relatively faraway loads.

TABLE 6. Single-objective ORPD evaluated cases with time-varying demand and uncertain renewable power.

Scenario no.	% Loading P_d	Wind power (MW)	PV power (MW)	Scenario probability, Δ_{sc}	Scenario-based P_{loss} (MW)	Scenario-based VD (p.u.)
1	60.293	20.272	45.919	0.001	1.128	0.054
2	76.831	59.697	50.000	0.001	1.106	0.063
3	69.559	47.819	50.000	0.001	1.056	0.056
4	77.134	72.882	32.753	0.003	1.078	0.068
5	49.093	75.000	8.967	0.001	1.308	0.041
6	65.263	30.473	39.245	0.001	1.110	0.052
7	67.261	37.673	10.293	0.119	1.356	0.056
8	92.929	47.757	17.170	0.001	3.469	0.088
9	42.659	7.439	0.000	0.007	0.886	0.039
10	72.131	12.845	0.000	0.489	3.241	0.067
11	68.524	49.523	30.726	0.008	0.964	0.057
12	66.030	0.000	28.439	0.009	2.291	0.062
13	66.065	29.118	35.921	0.002	1.147	0.057
14	67.521	23.378	50.000	0.001	1.318	0.054
15	61.892	36.394	1.401	0.003	1.241	0.056
16	74.331	31.077	8.343	0.119	2.283	0.063
17	68.012	28.586	14.024	0.090	1.594	0.058
18	59.917	19.798	21.776	0.017	1.172	0.047
19	72.927	18.497	37.419	0.001	1.930	0.066
20	66.075	25.136	26.451	0.007	1.332	0.054
21	65.005	51.068	16.376	0.045	0.935	0.058
22	62.978	47.738	24.265	0.014	0.836	0.059
23	72.318	31.078	19.107	0.028	1.758	0.064
24	98.525	0.000	9.026	0.003	8.920	0.113
25	79.921	12.810	3.665	0.029	4.247	0.076
Case 5				***EPL***	**2.4998**	
Case 6				***EVD***	**0.06314**	

TABLE 7. Multi-objective ORPD evaluated cases with time-varying demand and uncertain renewable power.

Scenario number	Scenario probability, Δ_{sc}	Objective value, LVD_{obj}	Scenario-based $P_{loss,sc}$	Scenario-based VD_{sc} (p.u.)
1	0.001	1.8659	1.2786	0.0587
2	0.001	1.8457	1.2006	0.0645
3	0.001	1.7215	1.1467	0.0575
4	0.003	1.8403	1.1931	0.0647
5	0.001	1.8946	1.4823	0.0412
6	0.001	1.7861	1.2127	0.0573
7	0.119	2.1111	1.5407	0.0570
8	0.001	4.7860	3.8620	0.0924
9	0.007	1.3751	1.0254	0.0350
10	0.489	4.2873	3.5870	0.0700
11	0.008	1.6867	1.0878	0.0599
12	0.009	3.1601	2.5572	0.0603
13	0.002	1.9522	1.3412	0.0611
14	0.001	2.0955	1.5059	0.0590
15	0.003	1.9141	1.3960	0.0518
16	0.119	3.2487	2.5371	0.0712
17	0.09	2.4069	1.8134	0.0594
18	0.017	1.9369	1.3406	0.0596
19	0.001	2.8247	2.1476	0.0677
20	0.007	2.0774	1.5093	0.0568
21	0.045	1.6515	1.0500	0.0601
22	0.014	1.4592	0.9519	0.0507
23	0.028	2.6591	1.9701	0.0689
24	0.003	10.8308	9.6683	0.1163
25	0.029	5.4893	4.6944	0.0795
Case 7			***EPL***	**2.7799**
			EVD	**0.06649**

The *EVD* results can also be examined in the same approach. With the lowest loading level (scenario 9), the bus voltage levels are maintained all over the network near to the desired 1.0 p.u. Due to the low current in scenario 9, a minimum aggregate VD is attained in this scenario. On the contrary, when network loading is maximum and the unavailability of wind turbine power in scenario 24, this leads to the highest aggregate VD of the system.

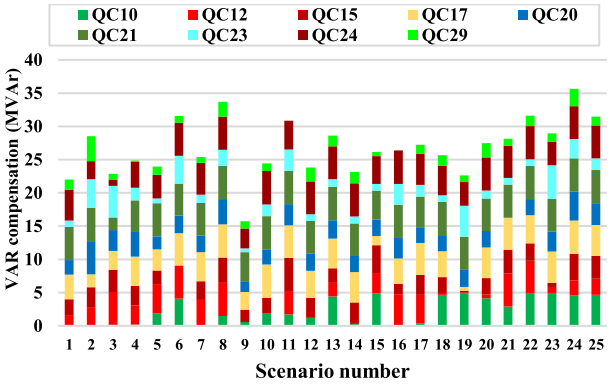

FIGURE 17. Optimal VAR compensator settings for all scenarios of Case 5.

Figure 12 and Figure 13 show the optimal values of the control variables for all scenarios in Case 5 and Case 6, respectively. Generally, the values of generator buses voltage in Case 5 are higher than those in Case 6. It is noted that bus#11 has the highest value of voltage setting, especially in Case (6) because it is directly linked to the adjacent load buses without any parallel reactive power compensators.

Figure 14 displays the PQ buses voltage profiles of scenario 9 and scenario 24 for both Case (5) and Case (6).

TABLE 8. Single-objective ORPD evaluated cases with time-varying demand and uncertain renewable power.

Control Variables	CPVEIHBMO [77]	GSA[78]	PSO[21]	DE[79]	OGSA [69]	CLPSO [21]	GWO [80]	NGBW CA [30]	JS	AEFA	Rao-3
Generator voltage											
V1	0.9926	0.9600	1.0853	1.0336	1.0350	1.0332	1.0204	1.0215	1.0026	0.9965	1.005619
V4	1.0108	0.9620	1.0420	1.0474	1.0554	1.0550	1.0257	1.0431	1.0332	1.0324	1.041145
V6	1.0037	0.9729	1.0805	1.0316	1.0301	0.9754	1.0208	1.0312	1.0256	1.0230	1.031482
V8	0.9976	1.0570	0.9683	1.0334	1.0175	0.9669	1.0419	1.0539	1.0377	1.0101	1.04171
V10	1.0215	1.0885	1.0756	1.0347	1.0250	0.9811	1.0413	1.0271	1.0579	0.9948	1.055457
V12	1.0093	0.9630	1.0225	1.0433	1.0410	1.0092	1.0232	1.0316	1.0276	1.0193	1.026048
V15	1.0075	1.0127	1.0786	1.0266	0.9973	0.9787	1.0207	1.0129	1.0197	0.9944	1.025839
V18	1.0259	1.0069	1.0498	1.0272	1.0047	1.0799	1.0270	1.0075	1.0271	0.9955	1.026774
V19	0.9943	1.0003	1.0776	1.0307	0.9899	1.0805	1.0204	1.0102	1.0198	0.9888	1.021509
V24	1.0179	1.0105	1.0827	1.0319	1.0287	1.0286	1.0137	1.0208	1.0255	0.9981	1.034654
V25	1.0177	1.0102	0.9564	1.0435	1.0600	1.0307	1.0270	1.0531	1.0588	1.0029	1.059846
V26	0.9990	1.0401	1.0809	1.0104	1.0855	0.9877	1.0386	0.9941	1.0593	1.0409	1.06
V27	1.0084	0.9809	1.0874	1.0189	1.0081	1.0157	1.0188	1.0291	1.0259	0.9798	1.031847
V31	0.9838	0.9500	0.9608	1.0481	0.9948	0.9615	1.0138	1.0275	1.0194	0.9819	1.021502
V32	0.9827	0.9552	1.1000	1.0215	0.9993	0.9851	1.0135	1.0201	1.0231	0.9826	1.029159
V34	1.0065	0.9910	0.9611	1.0277	0.9958	1.0157	1.0261	1.0014	1.0223	1.0170	1.047777
V36	1.0190	1.0091	1.0367	1.0254	0.9835	1.0849	1.0261	1.0412	1.0201	1.0150	1.04616
V40	1.0267	0.9505	1.0914	1.0224	0.9981	0.9830	1.0125	1.04	1.0272	1.0008	1.029714
V42	0.9865	0.9500	0.9701	1.0226	1.0068	1.0516	1.0233	1.0512	1.0218	1.0018	1.026529
V46	1.0084	0.9814	1.0390	1.0245	1.0355	0.9754	1.0272	1.017	1.0249	1.0112	1.028834
V49	1.0035	1.0444	1.0836	1.0426	1.0333	0.9838	1.0401	1.051	1.0376	1.0188	1.040376
V54	0.9806	1.0379	0.9764	1.0135	0.9911	0.9637	1.0230	1.0392	1.0224	0.9535	0.989651
V55	0.9969	0.9907	1.0103	1.0153	0.9914	0.9716	1.0221	1.0331	1.0186	0.9505	0.987586
V56	0.9881	1.0333	0.9536	1.0131	0.9920	1.0250	1.0226	1.0372	1.0192	0.9523	0.988918
V59	1.0197	1.0099	0.9672	1.0405	0.9909	1.0003	1.0379	1.0564	1.0275	0.9863	1.030353
V61	0.9956	1.0925	1.0938	1.0249	1.0747	1.0771	1.0241	1.0565	1.0257	1.0056	1.058546
V62	1.0064	1.0393	1.0978	1.0161	1.0753	1.0480	1.0199	1.0489	1.0241	1.0055	1.050738
V65	0.9883	0.9998	1.0892	1.0414	0.9814	0.9684	1.0465	1.0435	1.0495	1.0431	1.059397
V66	1.0101	1.0355	1.0861	1.0563	1.0487	0.9648	1.0378	1.0435	1.0509	1.0446	1.059996
V69	0.9931	1.1000	0.9665	1.0571	1.0490	0.9574	1.0501	1.0489	1.0556	1.0464	1.048068
V70	1.0127	1.0992	1.0783	1.0323	1.0395	0.9765	1.0243	1.0113	1.0256	1.0033	1.012537
V72	1.0145	1.0014	0.9506	1.0454	0.9900	1.0243	1.0187	1.0382	1.0264	1.0018	1.02606
V73	1.0174	1.0111	0.9722	1.0331	1.0547	0.9651	1.0397	0.9926	1.0279	1.0021	1.014203
V74	1.0025	1.0476	0.9713	1.0374	1.0167	1.0733	1.0170	0.9934	1.0009	0.9825	0.990476
V76	0.9842	1.0211	0.9602	1.0407	0.9972	1.0302	1.0080	1.0324	0.9930	0.9737	0.977726
V77	0.9914	1.0187	1.0781	1.0438	1.0071	1.0275	1.0192	1.0185	1.0201	1.0194	1.020787
V80	1.0257	1.0462	1.0788	1.0468	1.0066	0.9857	1.0329	1.0021	1.0312	1.0380	1.034043
V85	0.9876	1.0491	0.9568	1.0206	0.9893	0.9836	1.0224	1.0312	1.0255	1.0159	1.042649
V87	1.0213	1.0426	0.9642	1.0206	0.9693	1.0882	1.0361	1.0212	1.0258	1.0239	1.06
V89	1.0069	1.0955	0.9748	1.0436	1.0527	0.9895	1.0558	1.0387	1.0425	1.0271	1.059856
V90	1.0298	1.0417	1.0248	1.0166	1.0290	0.9905	1.0290	1.0071	1.0261	0.9943	1.037478
V91	0.9839	1.0032	0.9615	1.0146	1.0297	1.0288	1.0127	0.9989	1.0215	0.9894	1.041481
V92	1.0021	1.0927	0.9568	1.0374	1.0353	0.9760	1.0360	1.0001	1.0250	1.0092	1.038338
V99	0.9853	1.0433	0.9540	1.0034	1.0395	1.0880	1.0297	1.0467	1.0296	1.0110	1.020295
V100	1.0281	1.0786	0.9584	1.0384	1.0275	0.9617	1.0360	1.0213	1.0340	1.0179	1.028325
V103	0.9802	1.0266	1.0162	1.0450	1.0158	0.9611	1.0232	1.0416	1.0313	1.0131	1.013428
V104	1.0187	0.9808	1.0992	1.0459	1.0165	1.0125	1.0180	1.0174	1.0193	1.0022	0.990548
V105	1.0209	1.0163	0.9694	1.0383	1.0197	1.0684	1.0176	1.0223	1.0203	1.0015	0.985946
V107	1.0234	0.9987	0.9656	1.0141	1.0408	0.9769	1.0201	1.034	1.0247	0.9951	0.974218
V110	0.9842	1.0218	1.0873	1.0518	1.0288	1.0414	1.0207	1.0103	1.0259	1.0118	0.996554
V111	1.0000	0.9852	1.0375	1.0342	1.0194	0.9790	1.0261	1.0345	1.0322	1.0279	1.010089
V112	0.9930	0.9500	1.0920	1.0454	1.0132	0.9764	1.0066	1.016	1.0244	1.0013	0.982382
V113	1.0200	0.9764	1.0753	1.0281	1.0386	0.9721	1.0251	1.0181	1.0337	1.0074	1.036863
V116	1.0016	1.0372	0.9594	1.0508	0.9724	1.0330	1.0342	1.033	1.0365	1.0246	1.056441
Transformer tap ratio											
T8-5	1.0255	1.0659	1.0112	0.9937	0.9568	1.0045	1.0208	1.0051	0.9909	0.9878	0.971785
T26-25	0.9891	0.9534	1.0906	1.0081	1.0409	1.0609	1.0279	0.9614	1.0314	1.0398	1.047094
T30-17	0.9932	0.9328	1.0033	0.9789	0.9963	1.0008	1.0323	0.9961	1.0136	0.9923	0.987013
T38-37	0.9873	1.0884	1.0000	1.0169	0.9775	1.0093	1.0209	0.9523	1.0154	0.9618	0.962936
T63-59	0.9868	1.0579	1.0080	0.9973	0.9560	0.9922	1.0091	1.0521	1.0365	1.0591	1.011313
T64-61	1.0235	0.9493	1.0326	1.0258	0.9956	1.0074	1.0366	0.952	1.0343	1.0188	0.999329
T65–66	1.0090	0.9975	0.9443	1.0342	0.9882	1.0611	1.0301	0.9812	0.9776	1.0173	0.978985
T68–69	1.0075	0.9887	0.9067	0.9873	0.9251	0.9307	1.0234	0.951	1.0173	1.0031	0.955607
T81-80	0.9872	0.9801	0.9673	0.9930	1.0661	0.9578	1.0211	0.9754	0.9904	0.9263	1.009623
Capacitor bank											
QC5	0	0	0	−16.315	-0.3319	0	−39.76	−0.0723	-7.1679	-5.8878	-0.30522
QC34	6.0111	7.4600	9.3639	7.9425	0.0480	11.7135	13.7900	0.0483	7.7281	10.5145	13.98544
QC37	0	0	0	−9.4528	-0.2490	0	−24.73	−0.2390	-10.6387	-2.0182	0
QC44	6.0057	6.0700	9.3078	5.8755	0.0328	9.8932	9.9571	0.044	6.9277	8.1177	9.999989

TABLE 8. *(Continued.)* **Single-objective ORPD evaluated cases with time-varying demand and uncertain renewable power.**

QC45	3.0001	3.3300	8.6428	5.0360	0.0383	9.4169	9.8678	0.0372	6.9649	6.2519	1.36366
QC46	5.9838	6.5100	8.9462	3.5833	0.0545	2.6719	9.9186	0.0624	6.5598	7.1264	9.999985
QC48	3.9920	4.4700	11.8092	4.7675	0.0181	2.8546	14.8900	0.0172	9.5609	4.6386	14.97538
QC74	7.9862	9.7200	4.6132	6.9687	0.0509	0.5471	11.9720	0.0013	5.9780	9.7290	12
QC79	13.9892	14.2500	10.5923	10.2978	0.1104	14.8532	19.6490	0.0621	13.5997	13.4850	19.99572
QC82	17.9920	17.4900	16.4544	11.6685	0.0965	19.4270	19.8900	0.0463	11.5350	13.5978	19.66949
QC83	4.0009	4.2800	9.6325	4.0756	0.0263	6.9824	9.9515	0.056	5.1837	5.4863	9.991201
QC105	10.9825	12.0400	8.9513	5.0313	0.0442	9.0291	19.9680	0.0653	8.3469	10.2112	19.96196
QC107	2.0251	2.2600	5.0426	3.0884	0.0085	4.9926	5.9136	0.0072	2.9259	4.1279	3.156209
QC110	2.0272	2.9400	5.5319	2.6946	0.0144	2.2086	5.8834	0.0108	3.3661	2.2775	5.473934
Objective function											
P_{Loss} (MW)	124.098	127.76	131.99	122.3603	126.99	130.96	120.65	121.47	120.6093	126.7595	**118.4664**

TABLE 9. **The IEEE 30-bus system generators data.**

Bus no.	P_{min}	P_{max}	Q_{min}	Q_{max}	Settings of thermal units, P_G (MW)		
	(MW)	(MW)	(MVAr)	(MVAr)	Case 1, 2	Case 1a, 2a	Case 5, 6
1	50	200	-20	150	Swing	Swing	Swing
2	20	80	-20	60	75	80	75
5 (thermal)	15	50	-15	62.5	40	50	-
5 (wind)	0	75	-30	35	-	-	Variable
8 (thermal)	10	35	-15	48.7	30	20	-
8 (PV)	0	50	-20	25	-	-	Variable
11	10	30	-10	40	25	20	25

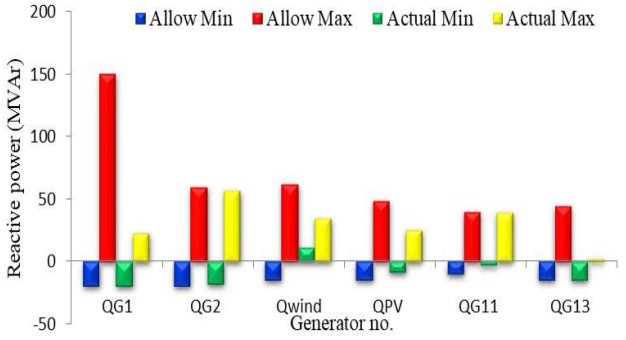

FIGURE 18. **Upper and lower reactive power values of the generators for all scenarios in Case 6.**

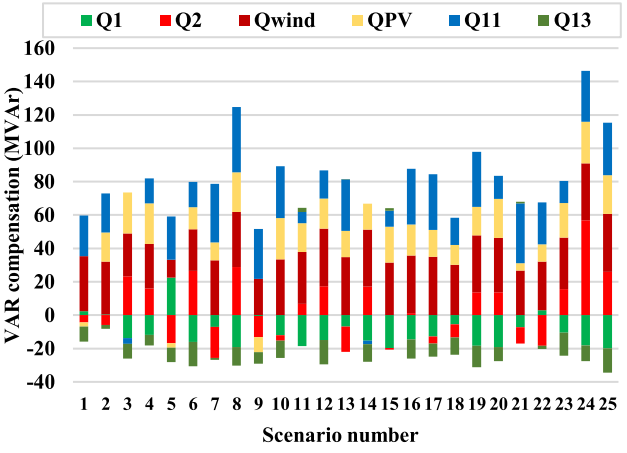

FIGURE 19. **Reactive power values of the generators for all scenarios of Case 6.**

Upper and lower ranges of reactive power contributions of all generators, actual ultimate and lowest values of reactive power across all scenarios for Case (5) and Case (6), respectively are displayed in Figure 15, and Figure 18. The reactive power values of the generators for all scenarios in Case (5) and Case (6) are shown in Figure 16, and Figure 19, respectively. Also, the optimal VAR compensator settings for all scenarios in Case (5) and Case (6) are displayed in Figure 17, and Figure 20, respectively.

E. MULTI-OBJECTIVE STOCHASTIC ORPD

In this subsection, both P_{loss} and VD minimization will be achieved as a multi-objective function (MO-ORPD). The weighted sum approach [27], [38], [75], is used to convert two objectives or more to a single objective, where each optimized function is multiplied by weight factor before summation of the cost functions [75], [76]. The cost function for MO-ORPD can be formulated as:

$$LVD_{obj} = \lambda_l P_{loss} + \lambda_{vd} \mathrm{VD} \tag{34}$$

where, P_{loss} and VD are evaluated using (2) and (3), respectively. The weight factor values are $\lambda_l = 1$ and $\lambda_{vd} = 10$.

Case (7) with the above-declared cost functions is executed on the modified 30-bus system. The conditions of this case are the same as in Cases (5) and (6). Table 7 lists the objective values (LVD_{obj}), scenario-based losses (P_{loss},), and voltage deviations (VD_{sc}). In this case, *EPL* and *EVD* values are higher than those values in Cases (5) and (6). The main

TABLE 10. The IEEE 57-bus system generators data.

Bus no.	P_{min} (MW)	P_{max} (MW)	Q_{min} (MVAr)	Q_{max} (MVAr)	Settings of thermal units, PG (MW) Case 3, 4	Case 3a, 4a
1	0	576	-140	200	Swing	Swing
2	30	100	-17	50	50	0
3	40	140	-10	60	60	40
6	30	100	-8	25	50	0
8	100	550	-140	200	400	450
9	30	100	-3	9	50	0
12	100	410	-150	155	300	310

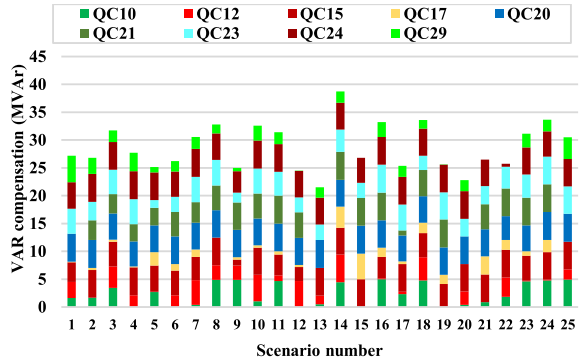

FIGURE 20. Optimal VAR compensator settings for all scenarios of Case 6.

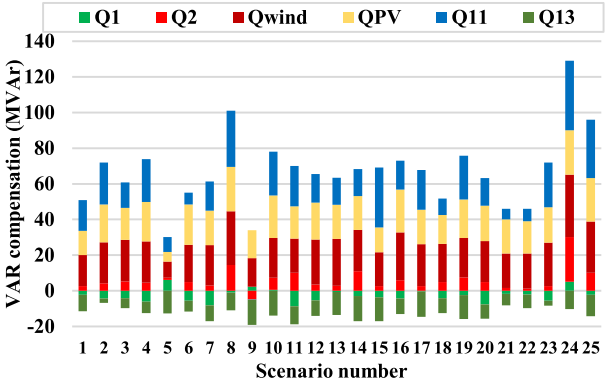

FIGURE 21. Reactive power values of the generators for all scenarios of Case 7.

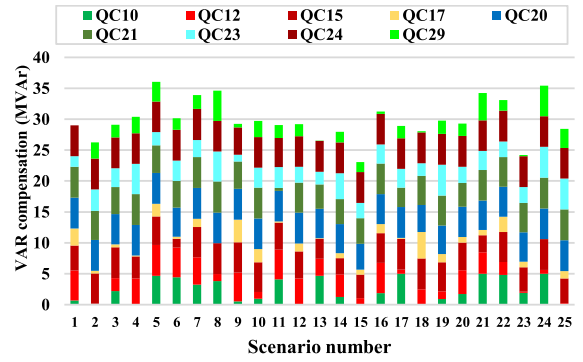

FIGURE 22. Optimal VAR compensator settings for all scenarios of Case 7.

reason is that the multi-objective optimization tries to achieve the best compromise solution of the constituting cost functions. Figure 21 displays the reactive power values of the

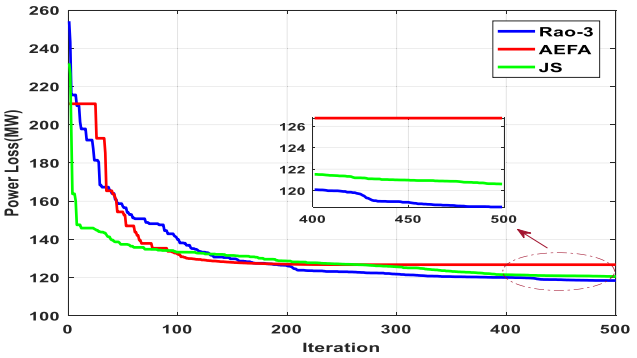

FIGURE 23. The convergence curves of Rao-3, AEFA, and JS algorithms for the studied case of P_{loss} for the 118-bus system (Case 8).

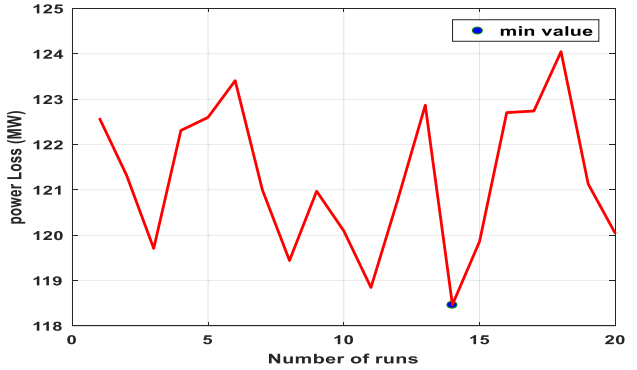

FIGURE 24. Values of the P_{loss} during 20 runs for the 118-bus system (Case 8).

generators for all scenarios of Case (7) while the optimal VAR compensator settings for all scenarios in Case (7) are shown in Figure 22.

F. TEST SYSTEM-4: IEEE 118-BUS TEST SYSTEM

The IEEE 118-bus test system consists of 54 generators, 9 tap changing transformers, 12 capacitor devices, and 2 reactor devices. The total system demand is 4242 MW [62]. Table 6 presents the optimal settings of control variables corresponding to the best value of real power losses. In this table, the solutions obtained by Rao-3 are better than those obtained by other metaheuristics algorithms. Figure 9 depicts the convergence characteristics of the proposed Rao-3, JS, and AEFA algorithms. Figure 5 displays the values of the power

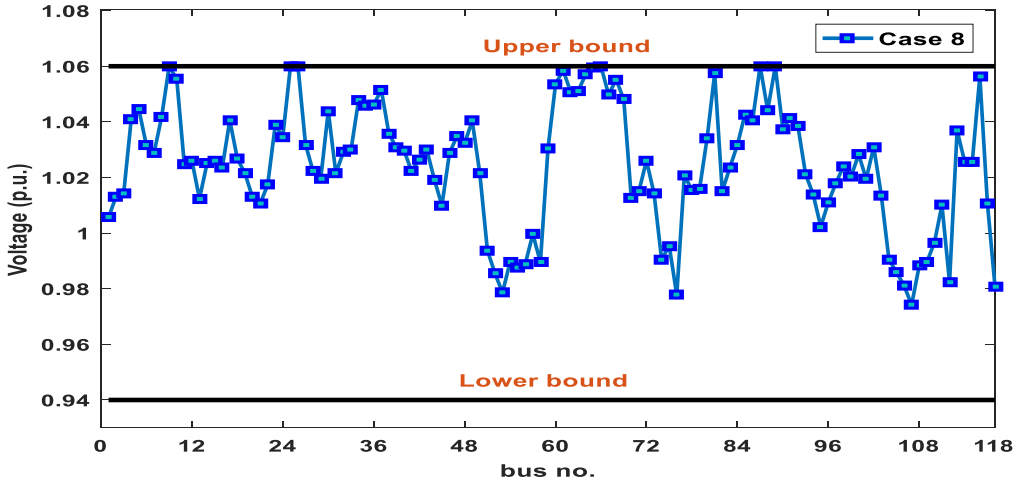

FIGURE 25. Voltage profiles of Load buses for the 118-bus system (Case 8).

TABLE 11. Designated scenarios and corresponding parameters for the scenarios.

Items	30-bus system				57-bus system	
	standard configuration		Adapted configuration		standard configuration	
	Number	Info	Number	Info	Number	Info
Buses	30	Table S.1 (Supp. doc.)	30	Variable load	57	[62]
Branches	41	[62]	41	[62]	80	[62]
Thermal generators	6	Buses: 1 (swing), 2, 5, 8, 11 and 13	4	Buses: 1 (swing), 2, 11 and 13	7	Buses: 1 (swing), 2, 3, 6, 8, 9 and 12
Wind generator	-		1	Bus 5	-	
PV unit	-		1	Bus 8	-	
Shunt VAR compensation	9	Buses: 10, 12, 15, 17, 20, 21, 23, 24 and 29	9	Buses: 10, 12, 15, 17, 20, 21, 23, 24 and 29	3	Buses: 18, 25 and 53
Transformer with tap changer	4	Branches: 11, 12, 15 and 36	4	Branches: 11, 12, 15 and 36	17	Branches: 19, 20, 31, 35, 36, 37, 41, 46, 54, 58, 59, 65, 66, 71, 73, 76 and 80
Control variables	19	-	19	-	27	-
Connected load	-	283.4 MW, 126.2 MVAr	-	Variable	-	1250.8 MW, 336.4 MVAr
Load bus voltage range allowed	24	[0.95 – 1.05] p.u.	24	[0.95 – 1.05] p.u.	50	[0.94 – 1.06] p.u.

loss during 20 runs for the 118-bus system. Figure 9 shows the voltage profile of PQ buses of the IEEE 118-bus system obtained by the proposed Rao-3.

VI. CONCLUSION

In this research, a new application for the Rao-3 algorithm has been proposed to solve the non-linear optimal reactive power dispatch problem. The integration of wind and solar energy generation systems as the most applied technologies for RES has been considered. In addition, the time-varying load and uncertainties of wind and solar energy resources have been investigated. Deterministic ORPD solutions for two standard systems (IEEE 30-bus and 57-bus) with only thermal generators have been performed in the first section of this paper. Afterward, stochastic ORPD solution in case of considering time-varying load, the uncertainty of wind and solar PV units have been considered by a scenario-based approach for the adapting 30-bus system. Various scenarios were created by Monte Carlo simulations. *EP*, and *EVD* values have been calculated with the optimization of network parameters under several scenarios of load demands, wind power, and PV power. Finally, Deterministic ORPD

TABLE 12. Limit setting for control variables of IEEE 118-bus system.

Variables	Lower limit	Upper limit
Voltages for generator bus	0.94 p.u	1.06 p.u
Voltages for load bus	0.95 p.u	1.05 p.u
Tap setting	0.9 p.u	1.1 p.u
QC5	−40 MVar	0 MVar
QC34	0 MVar	14 MVar
QC37	−15 MVar	0 MVar
QC44	0 MVar	10 MVar
QC45	0 MVar	10 MVar
QC46	0 MVar	10 MVar
QC48	0 MVar	10 MVar
QC74	0 MVar	12 MVar
QC79	0 MVar	20 MVar
QC82	0 MVar	20 MVar
QC83	0 MVar	10 MVar
QC105	0 MVar	20 MVar
QC107	0 MVar	6 MVar
QC110	0 MVar	6 MVar

solutions for the standard IEEE 118-bus with only thermal generators have been performed. The results provided the effectiveness and superiority of the proposed single-objective and multi-objective algorithms in solving the deterministic and stochastic ORPD problem compared with two recent algorithms (AEFA and JS) and other optimization algorithms used for the same problem. They readily lead the search process towards the feasible zone and subsequently ensure quick convergence to the global optimal solution.

APPENDIX

See Tables 9–12.

ACKNOWLEDGMENT

The authors thank the support of the National Research and Development Agency of Chile (ANID), ANID/Fondap/15110019.

REFERENCES

[1] S. Abdel-Fatah, M. Ebeed, S. Kamel, and J. Yu, "Reactive power dispatch solution with optimal installation of renewable energy resources considering uncertainties," in *Proc. IEEE Conf. Power Electron. Renew. Energy (CPERE)*, Oct. 2019, pp. 118–122, doi: 10.1109/CPERE45374.2019.8980056.

[2] D. C. Londoño, W. M. Villa-Acevedo, and J. M. López-Lezama, *Assessment of Metaheuristic Techniques Applied to the Optimal Reactive Power Dispatch* (Communications in Computer and Information Science)vol. 1052, pp. 250–262, 2019, doi: 10.1007/978-3-030-31019-6_22.

[3] N. Chen, M. Ieee, and R. Jan, "Application of the fast Newton-Raphson economic dispatch and reactive powernoltage dispatch," *IEEE Trans. Energy Convers.*, vol. 10, no. 2, pp. 293–301, Jun. 1995.

[4] S. Granville, "Optimal reactive dispatch through interior point methods," *IEEE Trans. Power Syst.*, vol. 9, no. 1, pp. 136–146, Feb. 1994.

[5] L. D. B. Terra and M. J. Short, "Security-constrained reactive power dispatch," *IEEE Trans. Power Syst.*, vol. 6, no. 1, pp. 109–117, Feb. 1991.

[6] K. Lee, Y. Park, and J. Ortiz, "A united approach to optimal real and reactive power dispatch," *IEEE Trans. Power App. Syst.*, vol. PAS-104, no. 5, pp. 1147–1153, May 1985.

[7] V. H. Quintana and M. Santos-Nieto, "Reactive-power dispatch by successive quadratic programming," *IEEE Power Eng. Rev.*, vol. 9, no. 9, pp. 44–45, Sep. 1989.

[8] M. Ebeed, S. Kamel, and F. Jurado, *Optimal Power Flow Using Recent Optimization Techniques*. Amsterdam, The Netherlands: Elsevier, 2018.

[9] K. B. O. Medani, S. Sayah, and A. Bekrar, "Whale optimization algorithm based optimal reactive power dispatch: A case study of the Algerian power system," *Electr. Power Syst. Res.*, vol. 163, pp. 696–705, Oct. 2018, doi: 10.1016/j.epsr.2017.09.001.

[10] B. Zhao, C. X. Guo, and Y. J. Cao, "A multiagent-based particle swarm optimization approach for optimal reactive power dispatch," *IEEE Trans. Power Syst.*, vol. 20, no. 2, pp. 1070–1078, May 2005.

[11] S. Mouassa, T. Bouktir, and A. Salhi, "Ant lion optimizer for solving optimal reactive power dispatch problem in power systems," *Eng. Sci. Technol., Int. J.*, vol. 20, no. 3, pp. 885–895, Jun. 2017, doi: 10.1016/j.jestch.2017.03.006.

[12] T. Trung, N. Dieu, and N. Vo, *Improved Social Spider Optimization Algorithm for Optimal Reactive Power Dispatch Problem With Different Objectives*, vol. 32, no. 10. London, U.K.: Springer, 2020.

[13] Z. Li, Y. Cao, L. Van Dai, X. Yang, and T. T. Nguyen, "Finding solutions for optimal reactive power dispatch problem by a novel improved antlion optimization algorithm," *Energies*, vol. 12, no. 5, p. 2968, 2019.

[14] Q. H. Wu, Y. J. Cao, and J. Y. Wen, "Optimal reactive power dispatch using an adaptive genetic algorithm," *Int. J. Electr. Power Energy Syst.*, vol. 20, no. 8, pp. 563–569, Nov. 1998.

[15] A. A. Abou El-Ela, A. M. Kinawy, R. A. El-Sehiemy, and M. T. Mouwafi, "Optimal reactive power dispatch using ant colony optimization algorithm," *Electr. Eng.*, vol. 93, no. 2, pp. 103–116, Jun. 2011, doi: 10.1007/s00202-011-0196-4.

[16] B. Shaw, V. Mukherjee, and S. P. Ghoshal, "Solution of reactive power dispatch of power systems by an opposition-based gravitational search algorithm," *Int. J. Electr. Power Energy Syst.*, vol. 55, pp. 29–40, Feb. 2014, doi: 10.1016/j.ijepes.2013.08.010.

[17] S. M. Shaheen, M. A. El-Sehiemy, and A. R. Farrag, "A novel framework for power loss minimization by modified wind driven optimization algorithm," in *Proc. Int. Conf. Innov. Trends Comput. Eng.*, Aswan, Egypt, no. 1, 2018, pp. 344–349.

[18] W. S. Sakr, R. A. EL-Sehiemy, and A. M. Azmy, "Adaptive differential evolution algorithm for efficient reactive power management," *Appl. Soft Comput.*, vol. 53, pp. 336–351, Apr. 2017, doi: 10.1016/j.asoc.2017.01.004.

[19] W. Villa-Acevedo, J. López-Lezama, and J. Valencia-Velásquez, "A novel constraint handling approach for the optimal reactive power dispatch problem," *Energies*, vol. 11, no. 9, p. 2352, Sep. 2018, doi: 10.3390/en11092352.

[20] Q. H. Wu and J. T. Ma, "Power system optimal reactive power dispatch using evolutionary programming," *IEEE Trans. Power Syst.*, vol. 10, no. 3, pp. 1243–1249, Aug. 1995.

[21] K. Mahadevan and P. S. Kannan, "Comprehensive learning particle swarm optimization for reactive power dispatch," *Appl. Soft Comput.*, vol. 10, no. 2, pp. 641–652, Mar. 2010, doi: 10.1016/j.asoc.2009.08.038.

[22] W. Zhang and Y. Liu, "Multi-objective reactive power and voltage control based on fuzzy optimization strategy and fuzzy adaptive particle swarm," *Int. J. Electr. Power Energy Syst.*, vol. 30, no. 9, pp. 525–532, Nov. 2008, doi: 10.1016/j.ijepes.2008.04.005.

[23] C. Dai, W. Chen, Y. Zhu, and X. Zhang, "Seeker optimization algorithm for optimal reactive power dispatch," *IEEE Trans. Power Syst.*, vol. 24, no. 3, pp. 1218–1231, Aug. 2009.

[24] M. H. Sulaiman, M. I. M. Rashid, M. S. Bakar, M. R. Mohamed, A. Z. Ahmad, and O. Aliman, "Loss minimisation by optimal reactive power dispatch using cuckoo search algorithm," in *Proc. 3rd IET Int. Conf. Clean Energy Technol. (CEAT)*, no. 5, 2014, pp. 1–4.

[25] W. Yan, S. Lu, and D. C. Yu, "A novel optimal reactive power dispatch method based on an improved hybrid evolutionary programming technique," *IEEE Trans. Power Syst.*, vol. 19, no. 2, pp. 913–918, May 2004.

[26] A. H. Khazali and M. Kalantar, "Optimal reactive power dispatch based on harmony search algorithm," *Int. J. Electr. Power Energy Syst.*, vol. 33, no. 3, pp. 684–692, Mar. 2011, doi: 10.1016/j.ijepes.2010.11.018.

[27] B. Mandal and P. K. Roy, "Optimal reactive power dispatch using quasi-oppositional teaching learning based optimization," *Int. J. Electr. Power Energy Syst.*, vol. 53, pp. 123–134, Dec. 2013, doi: 10.1016/j.ijepes.2013.04.011.

[28] A. B. K. Chattopadhyay, "Solution of optimal reactive power flow using biogeography-based optimization," *Int. J. Electr. Comput. Eng.*, vol. 4, no. 3, pp. 621–629, 2010.

[29] S. Abdel-Fatah, M. Ebeed, and S. Kamel, "Optimal reactive power dispatch using modified sine cosine algorithm," in *Proc. Int. Conf. Innov. Trends Comput. Eng. (ITCE)*, Feb. 2019, pp. 510–514, doi: 10.1109/ITCE.2019.8646460.

[30] A. A. Heidari, R. A. Abbaspour, and A. R. Jordehi, "Gaussian bare-bones water cycle algorithm for optimal reactive power dispatch in electrical power systems," *Appl. Soft Comput.*, vol. 57, pp. 657–671, Aug. 2017, doi: 10.1016/j.asoc.2017.04.048.

[31] M. G. Gafar, R. A. El-Sehiemy, and H. M. Hasanien, "A novel hybrid fuzzy-JAYA optimization algorithm for efficient ORPD solution," *IEEE Access*, vol. 7, pp. 182078–182088, 2019, doi: 10.1109/ACCESS.2019.2955683.

[32] S. Abdel-Fatah, M. Ebeed, S. Kamel, and L. Nasrat, "Moth swarm algorithm for reactive power dispatch considering stochastic nature of renewable energy generation and load," in *Proc. 21st Int. Middle East Power Syst. Conf. (MEPCON)*, Dec. 2019, pp. 594–599.

[33] S. Kamel, S. Abdel-Fatah, M. Ebeed, J. Yu, K. Xie, and C. Zhao, "Solving optimal reactive power dispatch problem considering load uncertainty," in *Proc. IEEE Innov. Smart Grid Technol. Asia (ISGT Asia)*, May 2019, pp. 1335–1340, doi: 10.1109/ISGT-Asia.2019.8881322.

[34] P. P. Biswas, P. N. Suganthan, R. Mallipeddi, and G. A. J. Amaratunga, "Optimal reactive power dispatch with uncertainties in load demand and renewable energy sources adopting scenario-based approach," *Appl. Soft Comput.*, vol. 75, pp. 616–632, Feb. 2019, doi: 10.1016/j.asoc.2018.11.042.

[35] N. H. Khan, Y. Wang, D. Tian, R. Jamal, M. Ebeed, and Q. Deng, "Fractional PSOGSA algorithm approach to solve optimal reactive power dispatch problems with uncertainty of renewable energy resources," *IEEE Access*, vol. 8, pp. 215399–215413, 2020, doi: 10.1109/ACCESS.2020.3039571.

[36] M. Ebeed, A. Ali, M. I. Mosaad, and S. Kamel, "An improved lightning attachment procedure optimizer for optimal reactive power dispatch with uncertainty in renewable energy resources," *IEEE Access*, vol. 8, pp. 168721–168731, 2020, doi: 10.1109/access.2020.3022846.

[37] M. Ebeed, A. Alhejji, S. Kamel, and F. Jurado, "Solving the optimal reactive power dispatch using marine predators algorithm considering the uncertainties in load and wind-solar generation systems," *Energies*, vol. 13, no. 17, p. 4316, Aug. 2020.

[38] R.-H. Liang, J.-C. Wang, Y.-T. Chen, and W.-T. Tseng, "An enhanced firefly algorithm to multi-objective optimal active/reactive power dispatch with uncertainties consideration," *Int. J. Electr. Power Energy Syst.*, vol. 64, pp. 1088–1097, Jan. 2015, doi: 10.1016/j.ijepes.2014.09.008.

[39] M. Naidji and M. Boudour, "Stochastic multi-objective optimal reactive power dispatch considering load and renewable energy sources uncertainties: A case study of the adrar isolated power system," *Int. Trans. Electr. Energy Syst.*, vol. 30, no. 6, pp. 1–28, Jun. 2020, doi: 10.1002/2050-7038.12374.

[40] S. Shargh, B. K. Ghazani, B. Mohammadi-ivatloo, H. Seyedi, and M. Abapour, "Probabilistic multi-objective optimal power flow considering correlated wind power and load uncertainties," *Renew. Energy*, vol. 94, pp. 10–21, Aug. 2016, doi: 10.1016/j.renene.2016.02.064.

[41] R. Karuppiah, M. Martín, and I. E. Grossmann, "A simple heuristic for reducing the number of scenarios in two-stage stochastic programming," *Comput. Chem. Eng.*, vol. 34, no. 8, pp. 1246–1255, Aug. 2010, doi: 10.1016/j.compchemeng.2009.10.009.

[42] L. A. Zadeh, "Fuzzy sets," *Inf. Control*, vol. 8, no. 3, pp. 338–353, Jun. 1965.

[43] M. Aien, M. Rashidinejad, and M. Fotuhi-Firuzabad, "On possibilistic and probabilistic uncertainty assessment of power flow problem: A review and a new approach," *Renew. Sustain. Energy Rev.*, vol. 37, pp. 883–895, Sep. 2014, doi: 10.1016/j.rser.2014.05.063.

[44] M. Nazari-Heris and B. Mohammadi-Ivatloo, *Application of Robust Optimization Method to Power System Problems*. Amsterdam, The Netherlands: Elsevier, 2018.

[45] N. Sharma, "Stochastic techniques used for optimization in solar systems: A review," *Renew. Sustain. Energy Rev.*, vol. 16, no. 3, pp. 1399–1411, Apr. 2012, doi: 10.1016/j.rser.2011.11.019.

[46] Y.-H. Bui, A. Hussain, and H.-M. Kim, "Double deep *Q*-learning-based distributed operation of battery energy storage system considering uncertainties," *IEEE Trans. Smart Grid*, vol. 11, no. 1, pp. 457–469, Jan. 2020, doi: 10.1109/TSG.2019.2924025.

[47] A. Martinez-Mares, C. R. Fuerte-Esquivel, and S. Member, "A robust optimization approach for the interdependency analysis of integrated energy systems considering wind power uncertainty," *IEEE Trans. Power Syst.*, vol. 28, no. 4, pp. 3964–3976, Nov. 2013.

[48] R. Mallipeddi, S. Jeyadevi, P. N. Suganthan, and S. Baskar, "Efficient constraint handling for optimal reactive power dispatch problems," *Swarm Evol. Comput.*, vol. 5, pp. 28–36, Aug. 2012, doi: 10.1016/j.swevo.2012.03.001.

[49] S. M. Mohseni-Bonab and A. Rabiee, "Optimal reactive power dispatch: A review, and a new stochastic voltage stability constrained multi-objective model at the presence of uncertain wind power generation," *IET Gener., Transmiss. Distrib.*, vol. 11, no. 4, pp. 815–829, Mar. 2017, doi: 10.1049/iet-gtd.2016.1545.

[50] J. Hetzer, D. C. Yu, and K. Bhattarai, "An economic dispatch model incorporating wind power," *IEEE Trans. Energy Convers.*, vol. 23, no. 2, pp. 603–611, Jun. 2008, doi: 10.1109/TEC.2007.914171.

[51] P. P. Biswas, P. N. Suganthan, and G. A. J. Amaratunga, "Optimal power flow solutions incorporating stochastic wind and solar power," *Energy Convers. Manage.*, vol. 148, pp. 1194–1207, Sep. 2017, doi: 10.1016/j.enconman.2017.06.071.

[52] S. S. Reddy, P. R. Bijwe, and A. R. Abhyankar, "Real-time economic dispatch considering renewable power generation variability and uncertainty over scheduling period," *IEEE Syst. J.*, vol. 9, no. 4, pp. 1440–1451, Dec. 2015, doi: 10.1109/JSYST.2014.2325967.

[53] Y. M. Atwa, E. F. El-Saadany, M. M. A. Salama, and R. Seethapathy, "Optimal renewable resources mix for distribution system energy loss minimization," *IEEE Trans. Power Syst.*, vol. 25, no. 1, pp. 360–370, Feb. 2010.

[54] A. Soroudi, M. Aien, and M. Ehsan, "A probabilistic modeling of photo voltaic modules and wind power generation impact on distribution networks," *IEEE Syst. J.*, vol. 6, no. 2, pp. 254–259, Jun. 2012, doi: 10.1109/JSYST.2011.2162994.

[55] R. V. Rao, "Rao algorithms: Three metaphor-less simple algorithms for solving optimization problems," *Int. J. Ind. Eng. Comput.*, vol. 11, no. 1, pp. 107–130, 2020, doi: 10.5267/j.ijiec.2019.6.002.

[56] L. Wang, Z. Wang, H. Liang, and C. Huang, "Parameter estimation of photovoltaic cell model with Rao-1 algorithm," *Optik*, vol. 210, May 2020, Art. no. 163846, doi: 10.1016/j.ijleo.2019.163846.

[57] R. V. Rao and R. B. Pawar, "Constrained design optimization of selected mechanical system components using Rao algorithms," *Appl. Soft Comput.*, vol. 89, Apr. 2020, Art. no. 106141, doi: 10.1016/j.asoc.2020.106141.

[58] M. Premkumar, T. S. Babu, S. Umashankar, and R. Sowmya, "A new metaphor-less algorithms for the photovoltaic cell parameter estimation," *Optik*, vol. 208, Apr. 2020, Art. no. 164559, doi: 10.1016/j.ijleo.2020.164559.

[59] R. V. Rao and R. B. Pawar, "Quasi-oppositional-based Rao algorithms for multi-objective design optimization of selected heat sinks," *J. Comput. Design Eng.*, vol. 7, no. 6, pp. 830–863, Dec. 2020, doi: 10.1093/jcde/qwaa060.

[60] R. V. Rao and H. S. Keesari, "Rao algorithms for multi-objective optimization of selected thermodynamic cycles," *Eng. Comput.*, Mar. 2020, Art. no. 0123456789, doi: 10.1007/s00366-020-01008-9.

[61] E. N. K. and S. B. Ikizler, "Rao-3 algorithm for the weight optimization of reinforced concrete cantilever retaining wall," *Geomech. Eng.*, vol. 20, no. 6, pp. 527–536, 2020.

[62] *Power Systems Test Case Archive*, Univ. Washington, Seattle, WA, USA, 2020. Accessed: Sep. 30, 2020. [Online]. Available: https://labs.ece.uw.edu/pstca/

[63] A. Yadav, "AEFA: Artificial electric field algorithm for global optimization," *Swarm Evol. Comput.*, vol. 48, pp. 93–108, Aug. 2019, doi: 10.1016/j.swevo.2019.03.013.

[64] J.-S. Chou and D.-N. Truong, "A novel metaheuristic optimizer inspired by behavior of jellyfish in ocean," *Appl. Math. Comput.*, vol. 389, Jan. 2021, Art. no. 125535, doi: 10.1016/j.amc.2020.125535.

[65] A. Rajan and T. Malakar, "Exchange market algorithm based optimum reactive power dispatch," *Appl. Soft Comput.*, vol. 43, pp. 320–336, Jun. 2016, doi: 10.1016/j.asoc.2016.02.041.

[66] A. A. A. E. Ela, M. A. Abido, and S. R. Spea, "Differential evolution algorithm for optimal reactive power dispatch," *Electr. Power Syst. Res.*, vol. 81, no. 2, pp. 458–464, Feb. 2011, doi: 10.1016/j.epsr.2010.10.005.

[67] R. N. S. Mei, M. H. Sulaiman, Z. Mustaffa, and H. Daniyal, "Optimal reactive power dispatch solution by loss minimization using moth-flame optimization technique," *Appl. Soft Comput.*, vol. 59, pp. 210–222, Oct. 2017, doi: 10.1016/j.asoc.2017.05.057.

[68] G. Chen, L. Liu, Z. Zhang, and S. Huang, "Optimal reactive power dispatch by improved GSA-based algorithm with the novel strategies to handle constraints," *Appl. Soft Comput.*, vol. 50, pp. 58–70, Jan. 2017, doi: 10.1016/j.asoc.2016.11.008.

[69] B. Shaw, V. Mukherjee, and S. P. Ghoshal, "Solution of optimal reactive power dispatch by an opposition-based gravitational search algorithm," in *Proc. Int. Conf. Swarm, Evol., Memetic Comput.*, 2013, pp. 558–567.

[70] A. Rajan and T. Malakar, "Optimal reactive power dispatch using hybrid Nelder–Mead simplex based firefly algorithm," *Int. J. Electr. Power Energy Syst.*, vol. 66, pp. 9–24, Mar. 2015, doi: 10.1016/j.ijepes.2014.10.041.

[71] E. Naderi, H. Narimani, M. Fathi, and M. R. Narimani, "A novel fuzzy adaptive configuration of particle swarm optimization to solve large-scale optimal reactive power dispatch," *Appl. Soft Comput.*, vol. 53, pp. 441–456, Apr. 2017, doi: 10.1016/j.asoc.2017.01.012.

[72] M. Mehdinejad, B. Mohammadi-Ivatloo, R. Dadashzadeh-Bonab, and K. Zare, "Solution of optimal reactive power dispatch of power systems using hybrid particle swarm optimization and imperialist competitive algorithms," *Int. J. Electr. Power Energy Syst.*, vol. 83, pp. 104–116, Dec. 2016, doi: 10.1016/j.ijepes.2016.03.039.

[73] M. Ghasemi, S. Ghavidel, M. M. Ghanbarian, and A. Habibi, "A new hybrid algorithm for optimal reactive power dispatch problem with discrete and continuous control variables," *Appl. Soft Comput.*, vol. 22, pp. 126–140, Sep. 2014, doi: 10.1016/j.asoc.2014.05.006.

[74] S. M. Mohseni-Bonab, A. Rabiee, and B. Mohammadi-Ivatloo, "Multi-objective optimal reactive power dispatch considering uncertainties in the wind integrated power systems," in *Reactive Power Control in AC Power Systems*. Cham, Switzerland: Springer, 2017, pp. 475–513.

[75] P. P. Biswas, P. N. Suganthan, R. Mallipeddi, and G. A. J. Amaratunga, "Optimal power flow solutions using differential evolution algorithm integrated with effective constraint handling techniques," *Eng. Appl. Artif. Intell.*, vol. 68, pp. 81–100, Feb. 2018, doi: 10.1016/j.engappai.2017.10.019.
[76] N. Srinivas and K. Deb, "Muiltiobjective optimization using nondominated sorting in genetic algorithms," *Evol. Comput.*, vol. 2, no. 3, pp. 221–248, Sep. 1994, doi: 10.1162/evco.1994.2.3.221.
[77] A. Ghasemi, K. Valipour, and A. Tohidi, "Multi objective optimal reactive power dispatch using a new multi objective strategy," *Int. J. Electr. Power Energy Syst.*, vol. 57, pp. 318–334, May 2014, doi: 10.1016/j.ijepes.2013.11.049.
[78] S. Duman, Y. Sönmez, U. Guvenc, and N. Yorukeren, "Optimal reactive power dispatch using a gravitational search algorithm," *IET Gener., Transmiss. Distrib.*, vol. 6, no. 6, pp. 563–576, Jun. 2012. doi: 10.1049/iet-gtd.2011.0681.
[79] J. A. Lampinen, K. Price, and R. M. Storn, *Differential Evolution: A Practical Approach to Global Optimization*. Berlin, Germany: Springer-Verlag, 2005, doi: 10.1007/3-540-31306-0.
[80] M. H. Sulaiman, Z. Mustaffa, M. R. Mohamed, and O. Aliman, "Using the gray wolf optimizer for solving optimal reactive power dispatch problem," *Appl. Soft Comput.*, vol. 32, pp. 286–292, Jul. 2015, doi: 10.1016/j.asoc.2015.03.041.

MOHAMED H. HASSAN received the M.Sc. degree in electrical engineering from Cairo University, Egypt, in 2018. He is currently pursuing the Ph.D. degree in electrical engineering with Aswan University, Egypt. His research interests include optimization techniques, renewable energy, and smart grids.

SALAH KAMEL received the International Ph.D. degree from the University of Jaen, Spain, and Aalborg University, Denmark, in January 2014. He is currently an Associate Professor with the Electrical Engineering Department, Aswan University. He is also a Leader of the Power Systems research group, Advanced Power Systems Research Laboratory (APSR Lab), Aswan, Egypt. His research activities include power system analysis and optimization, smart grid, and renewable energy systems.

MAHMOUD A. EL-DABAH received the B.Sc., M.Sc., and Ph.D. degrees from the Faculty of Engineering, Al-Azhar University, Cairo, Egypt, in 2007, 2012, and 2016, respectively. He is currently a Professor Assistant with the Electrical Engineering Department, Faculty of Engineering, Al-Azhar University. His research interests include power system operation, control, and planning, applications of modern optimization techniques in electric power systems, renewable energy sources, power system stability, and distributed power generation.

TAHIR KHURSHAID (Member, IEEE) received the B.E. degree in electrical engineering from Jammu University, India, in 2011, the master's degree in power system engineering from Galgotias University, Greater Noida, India, in 2014, and the Ph.D. degree in electrical engineering from the Department of Electrical Engineering, Yeungnam University, South Korea. He is currently working as an Assistant Professor with the Department of Electrical Engineering, Yeungnam University. His research interests include power system protection, power system optimization, power system analysis and design, and power system deregulation.

JOSÉ LUIS DOMÍNGUEZ-GARCÍA (Member, IEEE) received the B.S. and M.S. degrees in industrial engineering in 2009, and the Ph.D. degree in electrical engineering in 2013. He was a Visiting Researcher with the Institute of Energy, Cardiff University, the University of Strathclyde, Glasgow, and Huddersfield University, U.K., in 2011, 2016, and 2018, respectively. In 2010, he joined IREC, as a Researcher, where he is currently acts as the Head of the Power Systems Group. He is also the General Coordinator of the H2020 COREWIND and INCITE H2020 MSCA ITN project as well as WP leader of others. His work deals with the grid integration of renewable energy sources, smart grids, and microgrids.